

# Deep Reinforcement Learning for Real-Time Drone Routing in Post-Disaster Road Assessment Without Domain Knowledge

Huatian Gong

School of Civil and Environmental Engineering, Nanyang Technological University, Singapore, huatian.gong@ntu.edu.sg

Jiuh-Biing Sheu

Department of Business Administration, National Taiwan University, Taiwan, jbsheu@ntu.edu.tw

Zheng Wang

School of Maritime Economics and Management, Dalian Maritime University, China, drwz@dlut.edu.cn

Xiaoguang Yang

The Key Laboratory of Road and Traffic Engineering of the Ministry of Education, Tongji University, China, yangxg@tongji.edu.cn

Ran Yan

School of Civil and Environmental Engineering, Nanyang Technological University, Singapore, ran.yan@ntu.edu.sg

Rapid post-disaster road damage assessment is critical for effective emergency response, yet traditional optimization methods suffer from excessive computational time and require domain knowledge for algorithm design, making them unsuitable for time-sensitive disaster scenarios. This study proposes an attention-based encoder-decoder model (AEDM) for real-time drone routing decision in post-disaster road damage assessment. The method employs deep reinforcement learning to determine high-quality drone assessment routes without requiring algorithmic design knowledge. A network transformation method is developed to convert link-based routing problems into equivalent node-based formulations, while a synthetic road network generation technique addresses the scarcity of large-scale training datasets. The model is trained using policy optimization with multiple optima (POMO) with multi-task learning capabilities to handle diverse parameter combinations. Experimental results demonstrate two key strengths of AEDM: it outperforms commercial solvers by 16–69% in solution quality and achieves real-time inference (1–2 seconds) versus 100–2,000 seconds for traditional methods. The model exhibits strong generalization across varying problem scales, drone numbers, and time constraints, consistently outperforming baseline methods on unseen parameter distributions and real-world road networks. The proposed method effectively balances computational efficiency with solution quality, making it particularly suitable for time-critical disaster response applications where rapid decision-making is essential for saving lives.

*Key words:* Road damage assessment, Drone routing decision, Deep reinforcement learning, Attention-based encoder-decoder, Network transformation

## 1. Introduction

In recent years, the frequency and intensity of both natural disasters (e.g., earthquakes, hurricanes, and wildfires) and man-made crises (e.g., conflicts) have increased significantly, posing severe threats to human lives, property, and economic stability (Avishan et al. 2023). For example, the 2011 Japan earthquake resulted in over 15,000 deaths and approximately \$235 billion in economic losses, while the 2023 Turkey-Syria earthquake caused more than 50,000 fatalities (Sun et al. 2022). Between 2016 and 2020, disasters affected over 602 million people globally (Yang et al. 2023). Timely post-disaster emergency responses that include the delivery of essential supplies such as food, water, and medical aid are critical for saving lives (Organization et al. 2000). However, these efforts are often hindered by uncertainties in transportation infrastructure disruptions immediately following a disaster. Such uncertainties encompass the extent of road network damage, current operability, and feasibility of short-term restoration. Thus, rapid assessment of road network damage is essential to mitigate this uncertainty and enable effective humanitarian interventions.

Unmanned aerial vehicles, or drones, have emerged as a transformative tool for post-disaster damage assessment, offering distinct advantages over traditional methods (Enayati et al. 2023, Shi et al. 2024, Steenbergen et al. 2025). Their ability to capture high-resolution imagery at lower operational costs than satellites or helicopters makes them well-suited for rapid deployment in disaster zones (Zhang et al. 2023). Equipped with advanced sensors such as high-definition cameras, drones can systematically collect detailed data on road network conditions, including damage type and severity (e.g., cracks, landslides or complete collapses), current trafficability, and feasibility of short-term repairs. For instance, during the 2013 Typhoon Haiyan response in the Philippines, drones rapidly mapped affected areas and identified blocked roads, enabling relief teams to prioritize clearance efforts (Turk 2014). In Nepal's 2015 earthquake recovery, thermal drones assisted in locating survivors and assessing hard-to-reach mountain roads, showcasing their versatility in complex terrains (Abuali and Ahmed 2025). In post-disaster scenarios, traditional transportation options like cars, motorcycles, and even pedestrian access often become impassable and hazardous (Zhang et al. 2023). Roads may be collapsed or blocked by landslides, making ground-based access extremely difficult or even life-threatening. Drones, however, can operate freely in such hazardous environments, bypassing damaged infrastructure to collect critical information (Enayati et al. 2023, Shi et al. 2024, Steenbergen et al. 2025). This agility is pivotal in disaster response, where time sensitivity means timely information can determine survival outcomes. Building on these validated applications, this study proposes deploying a fleet of drones for rapid post-disaster road damage assessment.

Post-disaster road damage assessment via drone encompasses two critical timeframes: 1) the duration required to determine the routes for road damage assessment, and 2) the time taken by each drone to traverse its designated route. The first timeframe focuses on rapidly determining drone routing paths to enable efficient drone deployment. Existing literature tends to rely on traditional methodologies, including heuristics (e.g., genetic algorithms and simulated annealing) or exact methods (e.g., branch-and-price and column generation), to solve this routing problem (Huang et al. 2013, Balcik and Yanıkoğlu 2020). However, these methods suffer from three key limitations. First, their computational time increases significantly with problem size, making them ill-suited for time-critical disaster scenarios where delays in providing solutions can be unacceptable (Luo et al. 2023, Liu et al. 2024b). Second, developing a universally efficient algorithm to cope with such a drone routing problem is challenging. Such methods typically require extensive domain-specific expertise to engineer problem-tailored heuristics or exact formulations, which leads to prohibitive development costs and prolonged deployment cycles. Third, the problem's constraints evolve rapidly with changing environments (Kwon et al. 2020, Liu et al. 2024b), thus necessitating frequent redesign of specialized algorithms.

Advancements in computer vision (CV) and large language models (LLMs) have revolutionized their respective fields: expert-driven manual feature engineering has been supplanted by automated end-to-end deep learning, enabling models to learn complex patterns and generalize across diverse scenarios without heavy human intervention (Brown et al. 2020, Radford et al. 2021, Luo et al. 2023, Zhou et al. 2024, Liu et al. 2024a, Berto et al. 2024, Huang et al. 2025). Drawing inspiration from this paradigm shift, this study adopts a similar philosophy by proposing a deep reinforcement learning (DRL) model. Like CV and LLM that autonomously extract meaningful representations from raw data, the DRL model eliminates the need for domain-specific algorithm design by learning optimal routing strategies directly from problem instances. This allows it to determine high-quality drone assessment routes in real time, adapting to varying disaster scenarios and outperforming traditional algorithms by a significant margin. The second timeframe ensures timely completion of assessments from route initiation to drone return. The proposed model explicitly incorporates this timeliness constraint, optimizing both route planning and completion time within a predefined limit.

To achieve the above objectives, this study presents three contributions:

- We propose an attention-based encoder-decoder model (AEDM) for real-time decision-making in drone assessment route planning. Unlike traditional methods that rely on domain knowledge for algorithm design, AEDM operates autonomously. Experimental results demonstrate that it outperforms commercial solvers by a significant margin, with improvements ranging from 16–69%. More crucially, AEDM maintains real-time solving capability for large-scale

problems. In contrast, commercial solvers fail to yield solutions within a reasonable time frame for such complex scenarios, highlighting the model's superiority in time-critical post-disaster assessment tasks.

- We propose a simple yet efficient network transformation approach. This method integrates two distinct networks into a unified structure, enabling the conversion of a link-based routing problem into an equivalent node-based routing problem.
- We propose a synthetic road network generation method tailored for DRL in road network-related problems. This method addresses the scarcity of real-world large-scale road network datasets suitable for training advanced learning models.

The paper is structured as follows: Section 2 reviews the relevant literature. Section 3 introduces the drone-based road network assessment problem. Section 4 presents a simple yet efficient network transformation approach. Section 5 proposes AEDM. Section 6 evaluates the model's performance. Finally, Section 7 provides a summary.

## 2. Related work

In prior road damage assessment practices, four primary approaches have been employed. The first approach entails field surveys, which consist of on-site investigative activities such as community mapping and transect walks (Maya 2013). While these methods can provide detailed data, they are time-consuming, labor-intensive, and often fail to deliver timely insights during the critical early phases of disaster response (Tatham 2009). The second approach relies on remote sensing and geographic information system-based methods. These utilize satellite imagery to rapidly identify impacted areas. However, satellite revisit intervals (ranging from days to weeks) and resolution constraints limit their capacity to support prompt responses and detect fine-grained damages (Bravo et al. 2019). The third approach makes use of traffic data and sensor networks. It leverages global positioning systems, cameras, and embedded sensors to infer real-time road conditions. Yet, the limited deployment of such sensors in remote or underdeveloped regions undermines their feasibility for large-scale disaster scenarios (Yang et al. 2023). The fourth and final approach features drones. Drones emerge as a highly promising solution, owing to their high mobility, rapid deployability, and ability to capture high-resolution data in hazardous environments (Agatz et al. 2018, Zhang et al. 2023).

Recent literature has explored drone applications in post-disaster assessment. For example, Huang et al. (2013) formulated an assessment routing problem focusing on minimizing the total response time for visiting affected communities. Balcik (2017) and Balcik and Yanıkoğlu (2020) extended this to optimize site selection and routing under uncertain travel conditions, using traditional optimization techniques such as mixed-integer linear programming (MILP) solvers, genetic

algorithms, or tabu search. However, these methods require significant computational time as problem size increases, making real-time deployment challenging. Oruc and Kara (2018) combined drones and ground vehicles to optimize the assessment process but constrained drone movement to the physical road network, limiting flexibility. Zhang et al. (2023) introduced a robust team-orienting model solved via a branch-and-price approach, which remains computationally intensive for larger problems. Meanwhile, Adsanver et al. (2025) applied a multistage framework for grid damage assessment, but their heuristic-based models exhibit increased solution time with problem complexity. Table 1 presents a comparative overview of these methods, highlighting key differences in solution approaches, computational performance, and reliance on domain knowledge. It shows that traditional methods, whether heuristic (e.g., genetic algorithms and tabu search) or exact (e.g., branch-and-price), exhibit solution time that increases significantly with problem size even for moderate scales (e.g., 100+ nodes) and inherently require extensive domain-specific expertise for algorithm design. In contrast, our proposed DRL-based approach achieves real-time performance while handling larger networks (up to 1,000 nodes) and eliminates the need for domain knowledge, addressing the critical time sensitivity and expertise barriers of disaster response.

Given the time sensitivity of disaster response, the determination of assessment routes for each drone post-disaster must be as rapid as possible, ideally in real time. Heuristic algorithms, which aim to balance computational efficiency and solution quality, exhibit three notable limitations: First, they require substantial domain expertise to design effective rules, rendering the process time-consuming and costly (Liu et al. 2022, Luo et al. 2023, Zhou et al. 2024, Liu et al. 2024a). Second, they lack flexibility when faced with environmental changes or varying problem types, necessitating frequent adjustments (Zhang et al. 2020, Berto et al. 2024). Third, while performing adequately on smaller-scale problems, they incur longer solution time for larger scenarios, reducing computational efficiency and making them ill-suited for real-time applications (Chen et al. 2022, Arishi and Krishnan 2023). As a complement to these existing approaches, this study specifically addresses the urgency of post-disaster assessment by proposing a DRL model that determines high-quality drone routing plans in real time without domain knowledge. Our approach leverages advances in artificial intelligence (AI) to overcome the scalability and flexibility limitations inherent in classical optimization and heuristic methods, thereby enabling real-time and efficient damage assessment in complex post-disaster environments.

### 3. Problem definition

In the immediate aftermath of a disaster, the highly uncertain extent of road network damage underscores the critical need to rapidly assess network usability before executing emergency supply deployments and evacuation efforts. This problem is formally framed as follows. Given a road

**Table 1 Comparison of Road Damage Assessment Methods and Solutions**

Authors	Assessment tools	Objectives	Solutions	Method	Case study size	Computational time	Domain knowledge
Huang et al. (2013)	Routes teams	Minimize the sum of arrival time at all nodes	Continuous approximation approach	Heuristic	10 and 20 teams	Increase significantly with the case size	Required
Balcik (2017)	Routes teams	Cover nodes with different characteristics in a balanced way	Tabu search	Heuristic	94 nodes	Increase significantly with the case size	Required
Balcik and Yanıkoğlu (2020)	Routes teams	Cover nodes with different characteristics in a balanced way under uncertain travel time	Tabu search	Heuristic	94 nodes	Increase significantly with the case size	Required
Oruc and Kara (2018)	Drones and motorcycles	Maximize the total value added by the assessment of road links and maximize the total profit generated by assessing points of interest (nodes)	Base route heuristic	Heuristic	44 nodes	Increase significantly with the case size	Required
Glock and Meyer (2020)	Drones	Maximize the total informativeness of sampled locations within drones flight time limits	Two-phase multistart adaptive large neighborhood search	Heuristic	Up to 625 nodes	Increase significantly with the case size	Required
Zhang et al. (2023)	Drones	Maximize the collected link informative reward within a predefined time limit	Branch-and-price algorithm	Exact	Up to 107 nodes	Increase significantly with the case size	Required
Yin et al. (2023)	Trucks and drones	Minimize sum of dispatching cost, transport cost, and worst penalty cost of tardiness under demand and travel time uncertainties	Branch-and-price-and-cut algorithm	Exact	Up to 45 nodes	Increase significantly with the case size	Required
Morandi et al. (2024)	Truck and drones	Maximize total collected prize from nodes (visited by truck or served by drones) within a predefined time limit	Branch-and-cut algorithm	Exact	Up to 50 nodes	Increase significantly with the case size	Required
Adsanver et al. (2025)	Drones	Maximize the total priority scores of the visited grids and penalizes deviations from the maximum coverage target	Variable neighborhood descent	Heuristic	Up to 148 nodes	Increase significantly with the case size	Required
This study	Drones	Maximize the collected link informative reward within a predefined time limit	DRL	Heuristic	Up to 1,000 nodes	<b>Real-time</b>	<b>Not required</b>

network modeled as a graph  $G = (N, A)$  (where  $N$  denotes the set of road nodes, encompassing intersections in urban settings or intersections/villages in rural contexts, and  $A$  represents the links between these nodes) and a fleet of drones, the objective is to determine the assessment routes for each drone. These routes aim to maximize the total value of damage-related information collected across the network links. Drones, outfitted with high-definition cameras, are deployed to evaluate the damage status of each link. Due to a drone's operating altitude of 120 meters and its visual range (forming a circular area with a radius of approximately 75–80 meters), simultaneously inspecting multiple roads is impractical even within urban environments (Zhang et al. 2023). Consequently, a bidirectional road link can only be assessed if a drone flies directly along it.

To expedite drone movement and accelerate the assessment process, drones are permitted to travel directly between nodes, bypassing the physical road network links. As illustrated in Figure 1, consider a road network  $G = (N, A)$  with  $|N| = 5$  and  $|A| = 4$ : a drone stationed at node 1 may either traverse a specific road link (e.g., link  $(1, 2)$ , denoted by the blue line) to assess its condition, or opt for a more direct path (e.g., the straight-line route from node 1 to node 2, shown as the red line) to reach node 2 swiftly. In the latter scenario, the drone would forgo evaluating link  $(1, 2)$  and instead proceed to assess subsequent links (e.g.,  $(2, 3)$ ). This dual-network framework comprises two distinct structures: the original road network  $G$ , where drones evaluate individual link damage, and a fully connected auxiliary network  $G' = (N, A')$ , in which every node is directly connected to all other nodes. The auxiliary network  $G'$  enables drones to bypass physical road links, facilitating faster transit between nodes to prioritize assessments of additional critical links. Thus, alongside the original road network  $G$ , the introduction of  $G'$  enhances traversal efficiency, balancing thorough damage assessment with time-sensitive operational needs.

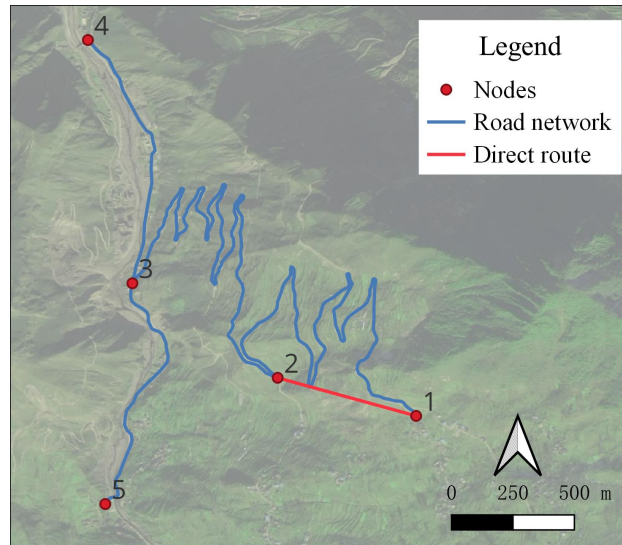


**Figure 1** Dual Network: Road Links (Assessment) vs. Direct Routes (Transit)

Let  $K$  denote the total number of drones, and  $Q$  represent the battery-imposed flight time limit for each drone. For the road network  $G = (N, A)$ , let  $(i, j) \in A$  denote an individual road link, where  $i, j \in N$  are road nodes. The time required for drone  $k$  to traverse link  $(i, j)$  while conducting a damage assessment is denoted as  $t_{ij}$ , which is computed based on the drone's flying speed and the physical length of  $(i, j)$ . Conversely,  $t'_{ij}$  represents the transit time between nodes  $i$  and  $j$  in the fully connected network  $G' = (N, A')$ , where the drone travels directly (without assessing  $(i, j)$ );  $t'_{ij}$  is typically shorter than  $t_{ij}$  due to the direct flight path. Let  $c_{ij}$  denote the damage information value obtained from assessing link  $(i, j)$ . Given the time sensitivity of post-disaster assessments,

$p_{\max}$  is defined as the maximum allowable duration for the entire assessment process. Under this constraint, each drone must complete its assigned assessments and return to its starting depot within  $p_{\max}$ .

The dual-network setup outlined above introduces a key challenge: ambiguities in distinguishing between road links (for assessment) and direct routes (for transit) when both connect the same pair of nodes. This ambiguity complicates the formulation of routing problems. To address this, the following section presents a network transformation approach that converts the link-based routing problem into an equivalent node-based formulation, resolving such ambiguities and enabling efficient computation.

## 4. Network transformation

### 4.1. Transformation method

This problem involves two distinct networks: the road network  $G = (N, A)$  and the fully connected node network  $G' = (N, A')$ . As visualized in Figure 2, (a) depicts the original road network  $G$ , where nodes are connected only via physical road links (e.g., edges between adjacent intersections), forming the structure where drones conduct damage assessments. (b) shows the fully connected auxiliary network  $G'$ , in which every node is directly linked to all other nodes, representing the direct transit paths drones can take to bypass road links. However, their integration into a dual-network configuration  $G'' = (N, A + A')$  introduces ambiguities, as shown in (c): multiple edges (road links vs. direct links) may connect the same pair of nodes, such as edge  $(1, 2)$ , which could represent either a road link from  $G$  or a direct link from  $G'$ .

To resolve this, existing studies have proposed transforming link-based routing networks into equivalent node-based ones. For example, Pearn (1988) converted a network with  $|A|$  links into an equivalent structure with  $3|A| + 1$  nodes, while Baldacci and Maniezzo (2006) and Longo et al. (2006) developed methods to reduce this to  $2|A| + 1$  nodes. However, these approaches often generate redundant links, increasing computational complexity. For the drone path planning problem, we adopt a traffic assignment method using intersection construction (Boyles et al. 2023) to reformulate the problem as a node-based routing task. As shown in Figure 3 (a), each road link  $(i, j) \in A$  is split by an artificial node  $p \in \mathcal{P}$ , creating two new links:  $(i, p)$  and  $(p, j)$ . This transforms the dual network  $G'' = (N, A + A')$  into a reduced network  $\bar{G} = (\bar{N}, \bar{A}) = (N \cup \mathcal{P}, 2A \cup A')$ , where  $|\mathcal{P}| = |A|$  (see Figure 3 (b)). In  $\bar{G}$ , the ambiguity of multiple edges between nodes is resolved: traversing  $(i, p)$  and  $(p, j)$  corresponds to assessing the original link  $(i, j)$ , while direct links in  $A'$  remain unchanged. By setting the information value of  $p$  as  $c_p = c_{ij}$  and splitting the traversal time as  $t_{ip} = t_{pj} = t_{ij}/2$ , the link-based routing problem is converted into a node-based one (examples in Figure 3 (c) and Figure 3 (d)). Notably, since  $|A| \ll |A'| + |N|$  (Boyles et al. 2023), this transformation adds only  $|A|$  nodes and  $|A|$  links, resulting in lower complexity compared to existing methods (Pearn 1988, Baldacci and Maniezzo 2006, Longo et al. 2006).



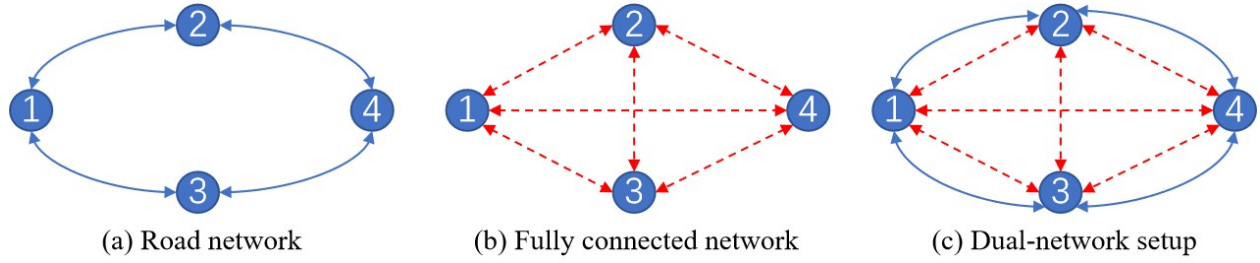


Figure 2 Dual Network Ambiguity: Overlapping Links Between Nodes

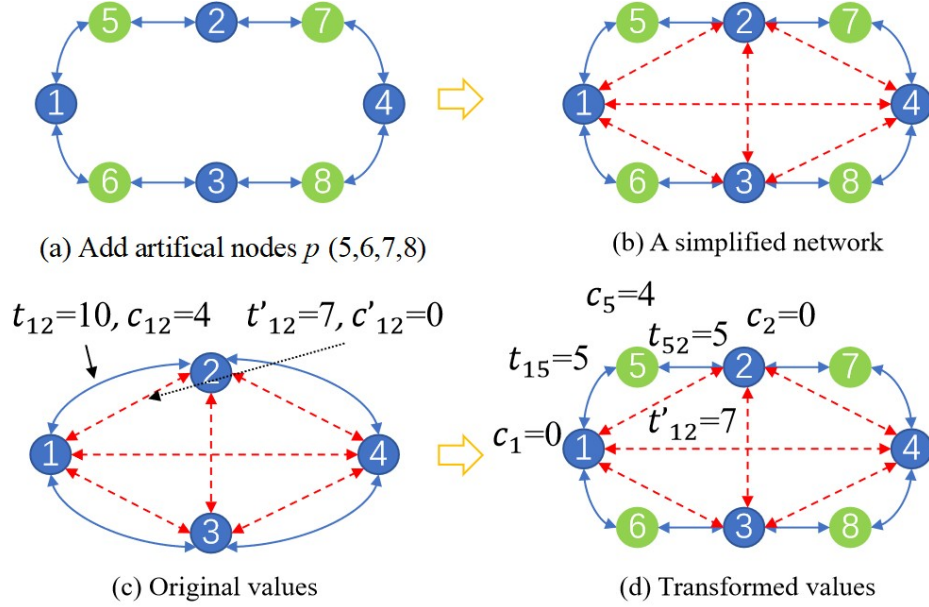


Figure 3 Link-to-Node Transformation via Artificial Nodes (where 5,6,7,and 8 are artificial nodes.)

#### 4.2. Coordinate generation

To systematically solve the problem, we address the coordinate generation for artificial nodes. In a given road network, geographical coordinates of original nodes are predefined (as shown in Figure 3 (c)), along with the corresponding road lengths, but coordinates of artificial nodes (e.g., nodes 5, 6, 7, 8 in Figure 3 (d)) are not. We propose a method to determine their coordinates as follows: Consider two nodes  $A(X_A, Y_A)$  and  $B(X_B, Y_B)$  in a 2D plane, with link  $(A, B)$  of length  $L$ . We aim to find coordinates of point  $C(X_C, Y_C)$  such that  $AC = BC = L/2$  and  $C$  lies on the perpendicular bisector of  $AB$  (see Figure 4). Compute the midpoint  $D$  of  $AB$ :  $X_D = (X_A + X_B)/2$ ,  $Y_D = (Y_A + Y_B)/2$ . The Euclidean distance between  $A$  and  $B$  is  $d_{AB} = \sqrt{(X_B - X_A)^2 + (Y_B - Y_A)^2}$ . Since  $C$  lies on the perpendicular bisector of  $AB$ , the direction vector of this bisector is  $(-(Y_B - Y_A), X_B - X_A)$ , and its unit normal vector is  $(-(Y_B - Y_A)/d_{AB}, (X_B - X_A)/d_{AB})$ . The coordinates of  $C$  are derived as (detailed derivation in Appendix 7):

$$X_C = \frac{X_A + X_B}{2} \mp \frac{\sqrt{L^2 - d_{AB}^2}}{2} \frac{Y_B - Y_A}{d_{AB}} \quad (1)$$

$$Y_C = \frac{Y_A + Y_B}{2} \pm \frac{\sqrt{L^2 - d_{AB}^2}}{2} \frac{X_B - X_A}{d_{AB}} \quad (2)$$

This yields two symmetric solutions for  $C$ , which lie on either side of the perpendicular bisector of  $AB$ . One solution is uniformly selected as the coordinate of  $C$ . Using this method, distances between nodes are computed as 2D Euclidean distances, simplifying the generation of subsequent training instances.

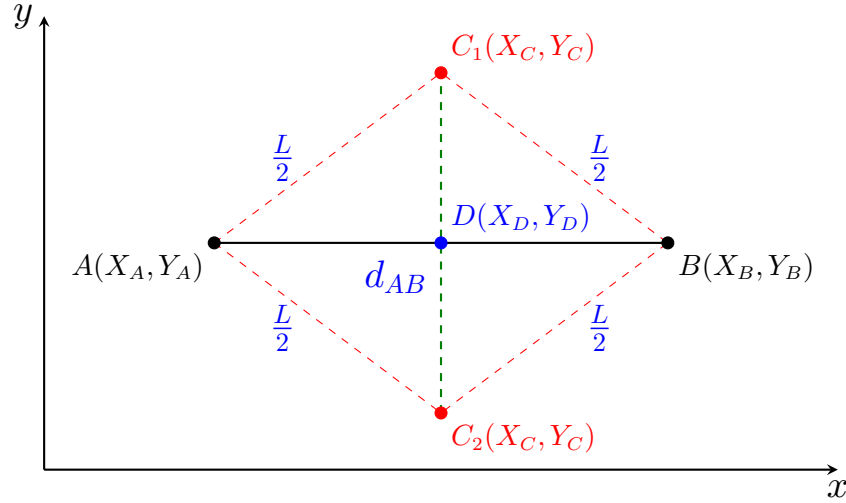


**Figure 4** Artificial Node Coordinate Calculation: Perpendicular Bisector Method

A key insight is that, via the proposed transformation (converting link-based routing to node-based routing), this drone routing problem resembles the orienteering problem (OP)—where nodes have prizes, and the goal is to maximize total collected prizes while keeping route length within a maximum limit (Gunawan et al. 2016, Kool et al. 2018, Zhang et al. 2023). However, critical differences exist as listed below, precluding direct application of existing OP algorithms. First, original nodes in  $N$  carry no information value, while artificial nodes in  $\mathcal{P}$  (representing road links) do. Second, in the transformed network  $\bar{G}$ , all nodes in  $N$  are mutually connected, but artificial nodes in  $\mathcal{P}$  are isolated from each other—each connects only to two specific nodes in  $N$ . Third, and most notably, artificial nodes in  $\mathcal{P}$  are exclusive: each can be visited by only one drone (as a road link’s information value is collected once), whereas nodes in  $N$  (valueless) can be revisited. For example, in Figure 3 (b) with four drones (each limited to one link by time constraints), if nodes 2 and 3 were non-revisitable, only two links’ information could be collected—suboptimal compared to four with revisits allowed. Additionally, revisits enable loops in drone paths: in Figure 5, a single drone’s optimal route (1,5,2,3,7,2,6,4) includes a loop (2,3,7,2), which would be impossible under non-revisitable constraints. This contrasts with OP’s Miller-Tucker-Zemlin (MTZ) constraints (Miller

et al. 1960), which prohibit cycles to ensure path continuity. These structural differences mean existing OP algorithms (exact or heuristic) cannot be directly applied. This highlights a common limitation of traditional algorithmic solutions: even minor modifications to the problem structure often require substantial redesign, which can be time-consuming and heavily reliant on expert domain knowledge. Moreover, in disaster-response scenarios where real-time decision-making is critical, there is an urgent need for methods that can deliver high-quality solutions as swiftly as possible, ideally in real time. In the following sections, we present a novel approach designed to tackle these challenges.

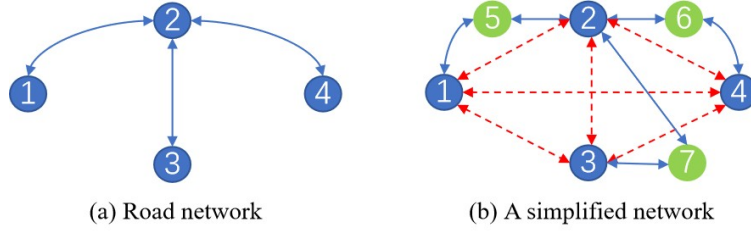


**Figure 5** Drone Path with Allowable Loops

## 5. Attention-based encoder-decoder model

To address the real-time solution requirement and eliminate the need for domain knowledge in algorithm design, we propose a learning-based framework, where a deep neural network is employed to map problem instance input data (denoted as vector  $\mathbf{x}$ ) to a valid solution (denoted as vector  $\mathbf{y}$ ). Given the absence of large-scale labeled training data  $(\mathbf{x}, \mathbf{y})$  for this novel problem—a common challenge for many emerging combinatorial optimization problems—we adopt reinforcement learning (RL) to train the deep neural network, enabling real-time inference without domain-specific expertise.

Formally, the problem is modeled as follows: for a given road network instance  $s$ , the network transformation method results in a road network with  $|\bar{N}|$  nodes. The task involves dispatching  $K$  drones to visit nodes in the transformed network  $\bar{G}$ , with the primary objective of maximizing the total information value collected, subject to the constraints that each drone has the battery flight time limit  $Q$  and the maximum allowable time for assessment  $p_{\max}$ . The solution is represented by a route set  $\pi = (\pi^1, \pi^2, \dots, \pi^K)$ , where  $\pi^k$  denotes the sequential path of nodes visited by the  $k$ -th drone. We propose AEDM that defines a stochastic policy  $p_\theta(\pi|s)$  to determine a route set solution  $\pi$  for a given road network instance  $s$ . This policy is factorized and parameterized by  $\theta$  as follows:

$$p_\theta(\pi|s) = \prod_{k=1}^K p_\theta(\pi^k|s, \pi^{1:k-1}) \quad (3)$$

where  $\pi^{1:k-1}$  denotes the set of paths constructed by the first  $k-1$  drones, affecting the current state when generating the  $k$ -th drone's path. Expanding further, for each path  $\pi^k = (\pi_1^k, \pi_2^k, \dots, \pi_t^k)$  where each  $\pi_t^k$  represents each node in the path  $\pi^k$ , its probability is expressed as:

$$p_\theta(\pi^k | s, \pi^{1:k-1}) = \prod_{t=1}^n p_\theta(\pi_t^k | s, \pi^{1:k-1}, \pi_{1:t-1}^k) \quad (4)$$

where  $n$  is the number of nodes in the drone's path, and  $\pi_{1:t-1}^k$  represents the sequence of nodes visited by the  $k$ -th drone before the  $(t-1)$ -th step. The model computes  $p_\theta(\pi_t^k | s, \pi^{1:k-1}, \pi_{1:t-1}^k)$  by considering the current state of the drone, the status of visited nodes (from  $\pi^{1:k-1}$  and  $\pi_{1:t-1}^k$ ), and the characteristics of the current node. The overall architecture of the model is illustrated in Figure 6, with detailed descriptions of its components presented subsequently.

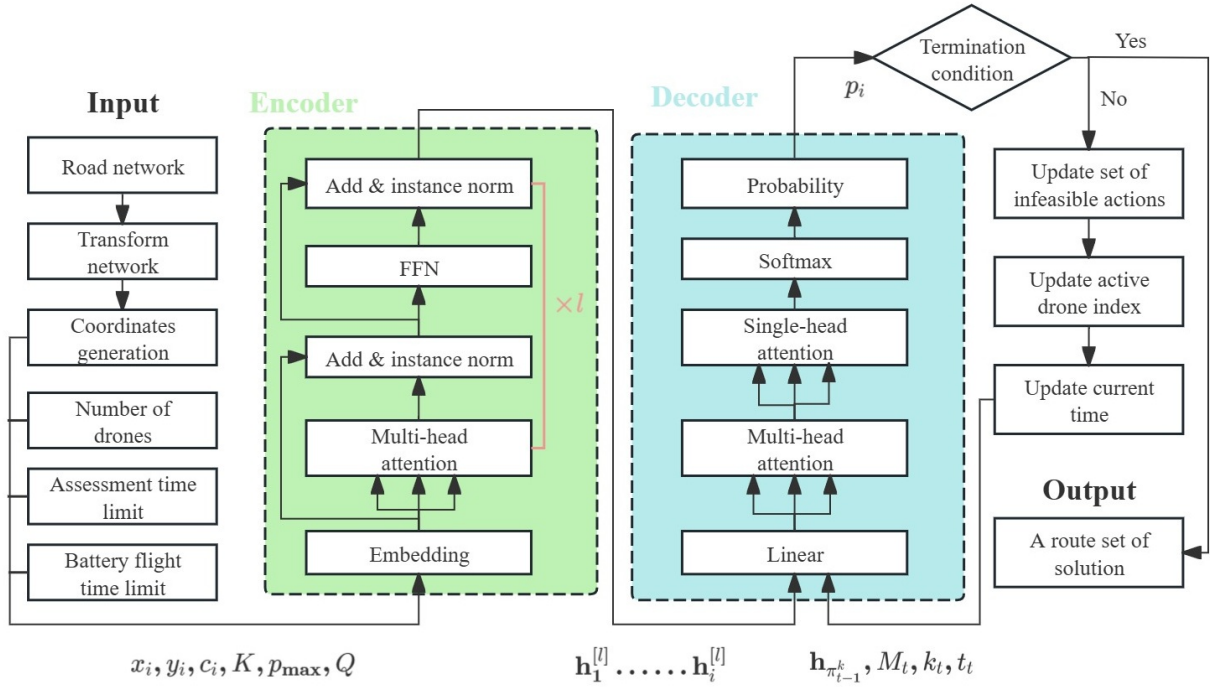


**Figure 6** Architecture of AEDM. The encoder processes road network coordinates and problem parameters through transformer layers to generate node embeddings. The decoder sequentially constructs drone routes using MHA and masking mechanisms to ensure feasible solutions.

### 5.1. Encoder

Leveraging the transformer architecture (Vaswani et al. 2017), the encoder employs embedding techniques to process and represent input data features. In the initial encoding stage, an embedding layer maps raw node features into a higher-dimensional latent space. Nodes are partitioned into two distinct categories:

- a) **Road network nodes** ( $\bar{N}$ ): Comprising original nodes ( $N$ ) and artificial nodes ( $\mathcal{P}$ ), each node  $i \in \bar{N}$  is defined by coordinates  $(x_i, y_i)$  and an information value  $c_i$ . Specifically,  $c_i = 0$  for  $i \in N$  and  $c_i > 0$  for  $i \in \mathcal{P}$  (encoding road link assessment values, as detailed in Section 4). Initial node embeddings are computed through linear transformation:

$$\mathbf{h}_i^{[0]} = [x_i, y_i, c_i] \mathbf{W}^{[0]} + \mathbf{b}^{[0]}, \quad \forall i \in \bar{N} \quad (5)$$

where  $[\cdot]$  denotes feature concatenation,  $\mathbf{W}^{[0]} \in \mathbb{R}^{3 \times d}$  and  $\mathbf{b}^{[0]} \in \mathbb{R}^d$  are learnable parameters, and  $\mathbf{h}_i^{[0]} \in \mathbb{R}^d$  represents the initial node representation.

- b) **Depot node** ( $o$ ): Functioning as the drones' origin and destination, its features incorporate coordinates  $(x_o, y_o)$  and global problem parameters  $(K, p_{\max}, Q)$ . These scalar parameters are embedded into the depot node via:

$$\mathbf{h}_o^{[0]} = [x_o, y_o, K, p_{\max}, Q] \mathbf{W}_o^{[0]} + \mathbf{b}_o^{[0]} \quad (6)$$

where  $\mathbf{W}_o^{[0]} \in \mathbb{R}^{5 \times d}$ ,  $\mathbf{b}_o^{[0]} \in \mathbb{R}^d$  are depot-specific learnable parameters, and  $\mathbf{h}_o^{[0]} \in \mathbb{R}^d$  is the initial depot embedding.

This heterogeneous embedding strategy differentiates node types and embeds global constraints into the depot's representation, forming a holistic input for subsequent attention-based processing. These embedding are then processed by  $l$  transformer layers (Kool et al. 2018), each consisting of two sublayers: a multi-head attention (MHA) sublayer and a node-wise fully connected feed-forward network (FFN) sublayer. Inspired by residual networks, a residual connection is employed to mitigate the issues of vanishing or exploding gradients in deep neural networks (He et al. 2016). Additionally, instance normalization (IN) is applied to accelerate training and enhance model performance. Mathematically, a transformer layer is defined as:

$$\bar{\mathbf{h}}_i = \text{IN}^{[l]} \left( \mathbf{h}_i^{[l-1]} + \text{MHA}^{[l]} \left( \mathbf{h}_1^{[l-1]}, \mathbf{h}_2^{[l-1]}, \dots, \mathbf{h}_i^{[l-1]} \right) \right) \quad (7)$$

$$\mathbf{h}_i^{[l]} = \text{IN}^{[l]} \left( \bar{\mathbf{h}}_i + \text{FFN}^{[l]} (\bar{\mathbf{h}}_i) \right) \quad (8)$$

After passing through  $l$  transformer layers, the resulting embedding vector  $\mathbf{h}_i^{[l]} \in \mathbb{R}^d$  is obtained for each node  $i$ , which are subsequently used as inputs to the decoder.

## 5.2. Decoder

The primary function of the decoder is to sequentially construct a solution by integrating the encoder's final output embeddings  $\mathbf{h}_i^{[l]}$  with the current state representation  $s_t$  at each time step  $t$ . A context embedding mechanism dynamically modulates the query space by combining the embedding of the current problem node with relevant state information. This context embedding

$\mathbf{h}_c^{(t)}$  is derived from a linear projection of concatenated features: the node embedding from the encoder's final layer ( $\mathbf{h}_i^{[l]}$ ) and dynamic state features including the current time  $d_t$  and the current index  $k_t$  of the active drone. Mathematically:

$$\mathbf{h}_c^{(t)} = \begin{cases} [\mathbf{h}_{\pi_{t-1}^k}, d_t, k_t] \mathbf{W}_c + \mathbf{b}_c & t \geq 1 \\ [\mathbf{h}_o, d_t, k_t] \mathbf{W}_c + \mathbf{b}_c & t = 0 \end{cases} \quad (9)$$

where  $\mathbf{h}_{\pi_{t-1}^k}$  denotes the final-layer encoder embedding of the node selected at the previous timestep  $\pi_{t-1}^k$ ;  $\mathbf{h}_o$  represents the depot embedding from the encoder's final layer;  $d_t$  and  $k_t$  capture the temporal state and active drone index respectively; and  $\mathbf{W}_c \in \mathbb{R}^{(d+2) \times d}$  and  $\mathbf{b}_c \in \mathbb{R}^d$  are learnable projection parameters. To enhance readability, we omit the encoder layer index, and in the decoder, all variables originating from the encoder refer to the output of the final encoder layer  $[l]$ . This context embedding formulation enables the decoder to maintain awareness of both the current solution state and operational constraints while generating subsequent actions. The explicit incorporation of temporal progression ( $d_t$ ) and drone index ( $k_t$ ) allows the model to dynamically adjust its decision policy based on the evolving solution characteristics.

Next, the MHA layer and a single-head attention (SHA) layer are applied, which are expressed as:

$$\bar{\mathbf{h}}_c^{(t)} = \text{MHA}(\mathbf{h}_c^{(t)}, \mathbf{h}_1, \mathbf{h}_2, \dots, \mathbf{h}_i, M_t) \quad (10)$$

$$\mathbf{u} = u_o, u_1, \dots, u_i = \text{SHA}(\bar{\mathbf{h}}_c^{(t)}, \mathbf{h}_1, \mathbf{h}_2, \dots, \mathbf{h}_i, M_t) \quad (11)$$

where  $M_t$  denotes the set of infeasible actions at the current time step  $t$ , which we will discuss later. To compute the output probability  $p_\theta(\pi_t^k | s, \pi^{1:k-1}, \pi_{1:t-1}^k)$  as given in equation (4), the probability of selecting node  $i$  at time step  $t$  is computed using the softmax function:

$$p_i = p_\theta(\pi_t^k | s, \pi^{1:k-1}, \pi_{1:t-1}^k) = \text{Softmax}(C \cdot \tanh(\mathbf{u})) \quad (12)$$

where  $C$  serves as a clipping parameter for the tanh function, enhancing solution exploration in the search space (Bello et al. 2016, Berto et al. 2024). Upon obtaining the probability distribution  $p_i$ , the current time step  $t$  is finalized, and the state is updated to  $t + 1$ , allowing the decoder to construct solutions autoregressively. The decoder terminates when either of the following conditions is met, yielding a feasible solution:

- a) All drones have been deployed, and the last drone returns to the depot;
- b) All nodes with damage information values (i.e., nodes in set  $\mathcal{P}$ ) have been visited, and the active drone returns to the depot.

Given that the detailed architectures of MHA, IN, FFN, and SHA represent mature techniques in large language models—thoroughly discussed in existing literature such as Vaswani et al. (2017),

Kool et al. (2018), Kwon et al. (2020), Luo et al. (2023), Zhou et al. (2024), Liu et al. (2024a), Berto et al. (2024)—this study refrains from redundant technical elaboration.

The following discusses the set of infeasible actions  $M_t$  that are masked (i.e., set  $u_i = -\infty$  for  $i \in \bar{N}$ ) at the current time step  $t$ :

- a) The next node is not connected to the current node at time step  $t$  in the transformed road network. This masking ensures that the decoder's output adheres to the routing rules of the road network.
- b) Nodes with damage information values (i.e., belonging to the set  $\mathcal{P}$ ) have been visited at the current time step  $t$ . This masking prevents redundant collection of damage information values from links.
- c) Each drone departs from the depot, collects a series of nodes, and must return to the depot within the specified assessment time limit  $p_{\max}$  or battery flight time limit  $Q$ . This masking enforces the flight time constraints for each drone. Due to the structure of the transformed road network—where nodes with damage information values are only connected to nodes without damage information values (not to the depot), and nodes without damage information values are fully connected—two cases are distinguished:
  - If the next node  $i$  to be visited belongs to  $N$  (i.e., no damage information value) and is connected to the depot, the node is masked if selecting  $i$  would cause the total flight time to exceed  $p_{\max}$  or  $Q$ , i.e.,  $i \in \left\{d_t + t_{\pi_{t-1}^k i} + t_{io} > p_{\max}\right\}$  or  $i \in \left\{d_t + t_{\pi_{t-1}^k i} + t_{io} > Q\right\}$ , where  $t_{\pi_{t-1}^k i}$  denotes the flight time from the previous node  $\pi_{t-1}^k$  to  $i$ , and  $t_{io}$  the flight time from the node  $i$  to depot  $o$ , as defined in Section 3.
  - If the next node  $i$  to be visited belongs to  $\mathcal{P}$  (i.e., with damage information value) and is not connected to the depot, an additional step is considered: the flight from  $i$  to the next depot-connected node. As each node  $i \in \mathcal{P}$  is connected to exactly two nodes in  $N$  with equal distances (see equations (1)–(2)), the node is masked if selecting  $i$  would cause the total flight time to exceed  $p_{\max}$  or  $Q$ , i.e.,  $i \in \left\{d_t + 2 \cdot t_{\pi_{t-1}^k i} + t_{io} > p_{\max}\right\}$  or  $i \in \left\{d_t + 2 \cdot t_{\pi_{t-1}^k i} + t_{io} > Q\right\}$ .

These mask mechanisms ensure adherence to the transformed network's structural constraints, prevents redundant information collection, and maintains operational time limits, guaranteeing feasible drone routing solutions.

Finally, the update rules for the active drone index  $k_t$  and current time  $d_t$  at the next time step  $t+1$  are as follows. For the active drone index  $k_{t+1}$ :

$$k_{t+1} = \begin{cases} k_t + 1 & \text{if the selected node } i \text{ is the depot } o \\ k_t & \text{if the selected node } i \text{ is not the depot} \end{cases} \quad (13)$$

This rule ensures that when a drone returns to the depot, the next drone in the fleet becomes active, facilitating sequential deployment of multiple drones. For the current time  $d_t$ :

$$d_{t+1} = \begin{cases} 0 & \text{if the selected node } i \text{ is the depot } o \\ d_t + t_{\pi_{t-1}^k i} & \text{if the selected node } i \text{ is not the depot} \end{cases} \quad (14)$$

Here,  $d_{t+1}$  resets to 0 when returning to the depot, reflecting the start of a mission for the next drone. When visiting a non-depot node  $i$ , the flight time  $t_{\pi_{t-1}^k i}$  from the previous node  $\pi_{t-1}^k$  to  $i$  is accumulated, maintaining the temporal consistency of the drone's mission timeline. These updates enable the decoder to dynamically manage multi-drone operations and enforce time constraints in the routing solution.

### 5.3. Training method

The stochastic policy in equation (4) is parameterized by  $\theta$  (encompassing all trainable variables of AEDM). For model optimization, policy gradient methods iteratively refine  $\theta$  via gradient estimation of the expected reward. While Kool et al. (2018) proposed the REINFORCE estimator—using a deterministic greedy rollout of the current best policy as baseline (updated periodically via paired t-test with  $\alpha = 5\%$ )—recent work by Kwon et al. (2020) showed that policy optimization with multiple optima (POMO) outperforms REINFORCE. Thus, we train AEDM using POMO.

Notably, our problem diverges from the original POMO in four key aspects. First, fixing  $K$  (drone number),  $p_{\max}$  (assessment time limit), and  $Q$  (battery constraint) reduces the problem to single-task learning—analogueous to training models for the fixed-vehicle number vehicle routing problem in Zhang et al. (2020). While simplifying training, this approach necessitates separate models for each parameter combination and requires matching models to combinations during deployment, which is inefficient. Inspired by multi-task capabilities of LLM, we advance AEDM as a multi-task framework: it is trained to handle diverse  $(K, p_{\max}, Q)$  combinations and, crucially, generalizes to unseen ones.

Second, two strategies exist for training such a multi-task model: (1) Directly mixing diverse parameter combinations within individual batches (Berto et al. 2024); (2) Training a fixed parameter set per batch, with varying combinations across successive batches (Zhou et al. 2024, Liu et al. 2024a). For our problem, decoder output lengths vary significantly across different combinations of  $K$ ,  $p_{\max}$ , and  $Q$ . For instance, with fixed  $p_{\max}$  and  $Q$ , the decoder output length for  $K = 4$  is nearly double that for  $K = 2$ . The latter accelerates training by ensuring near-uniform decoder output lengths across instances within each batch. Thus, we adopt the second strategy.

Third, RL aims to maximize the expected reward. However, within this multi-task learning framework where batches are trained on diverse parameter combinations, rewards vary accordingly. For instance, with other parameters fixed, rewards obtained under  $K = 2$  differ significantly from



those under  $K = 3$  or  $K = 4$ . This discrepancy arises because a larger number of drones (higher  $K$ ) can potentially collect more rewards by visiting additional nodes. To mitigate potential biases in the learning process, we propose a normalized reward strategy that combines exponentially moving average (EMA) with Z-score normalization, denoted as  $r_{\text{norm}}^{(pc)}$  (where  $pc$  represents a specific parameter combination). Specifically, we first compute the exponentially smoothed mean of rewards for each parameter combination over time:

$$\hat{\mu}_t^{(pc)} = (1 - \gamma) \cdot \hat{\mu}_{t-1}^{(pc)} + \gamma \cdot \mu_t^{(pc)} \quad (15)$$

where  $\mu_t^{(pc)}$  is the mean reward of the current batch for  $pc$ ,  $\hat{\mu}_{t-1}^{(pc)}$  is the smoothed mean from the previous batch, and  $\gamma \in [0, 1]$  (set to 0.25 following Berto et al. (2024)) controls the smoothing intensity, with initialization  $\hat{\mu}_1^{(pc)} = \mu_1^{(pc)}$ . We then calculate the exponentially smoothed variance to capture reward dispersion:

$$\hat{\sigma}_t^{(pc)} = (1 - \gamma) \cdot \hat{\sigma}_{t-1}^{(pc)} + \gamma \cdot \sigma_t^{(pc)} \quad (16)$$

where  $\sigma_t^{(pc)}$  is the variance of rewards in the current batch for  $pc$ , with initialization  $\hat{\sigma}_1^{(pc)} = \sigma_1^{(pc)}$ . The normalized reward is finally computed via Z-score transformation using the smoothed statistics:

$$r_{\text{norm}}^{(pc)} = \frac{r^{(pc)} - \hat{\mu}_t^{(pc)}}{\sqrt{\hat{\sigma}_t^{(pc)} + \epsilon}} \quad (17)$$

where  $\epsilon \approx 10^{-8}$  avoids division by zero. This approach simultaneously tracks changes in both mean and variance across batches, ensuring stable multi-task convergence by anchoring rewards to their historical trajectories within each parameter regime. As validated by the ablation study in Appendix 7, this normalization strategy outperforms alternatives such as batch-wise Z-score normalization and no normalization, minimizing optimality gaps and enhancing model stability across diverse parameter combinations.

Fourth, for POMO implementation (Kwon et al. 2020), we sample a solution set  $\Pi$ , where each  $\pi \in \Pi$  is determined by AEDM. Given the drone routing problem's nature—all drones depart from a shared depot—we enhance sample diversity by sequentially selecting  $N$  nodes from the transformed road network as a secondary visit set. Due to the network's structure: nodes with non-zero damage information values are disconnected from the depot, while those with zero values are connected. Thus,  $N$  nodes are sequentially chosen to form the secondary visit set for drones.

Combining these four modifications, parameter optimization is conducted using POMO with a shared baseline, formulated as follows. For notational simplicity, let  $R(\pi|s) = r_{\text{norm}}^{(pc)}$  denote the normalized reward function:

$$\nabla_{\theta} J(\theta) \approx \frac{1}{|\Pi|} \sum_{\pi \in \Pi} (R(\pi|s) - b(s)) \nabla_{\theta} \log p_{\theta}(\pi|s) \quad (18)$$

Here,  $s$  denotes a specific problem instance;  $R(\pi|s)$  represents the reward yielded by solution  $\pi$ , corresponding to the total collected damage information value. The shared baseline  $b(s)$  is defined as  $b(s) = \frac{1}{|\Pi|} \sum_{\pi \in \Pi} R(\pi|s)$ . Finally,  $p_\theta(\pi|s)$  denotes the aggregated selection probabilities of nodes at each decoder step. A summary of the AEDM training procedure is provided in Algorithm 1. Additionally, the model’s learning mechanism—transitioning from memorizing input parameters to reasoning about problem structures—is further validated by the t-distributed stochastic neighbor embedding (t-SNE) interpretability analysis in Appendix 7, which illustrates the evolutionary trajectory of features across encoder layers and confirms the effectiveness of the proposed training framework.

---

**Algorithm 1** POMO with Four Modifications for AEDM Training

---

- 1: **Input:** Total epochs  $E$ , iterations per epoch  $T$ , batch size  $B$ , parameter combinations  $\mathcal{C} = \{(K, p_{\max}, Q)\}$
  - 2: **Initialize:** Policy network parameters  $\theta$
  - 3: **for** epoch = 1 to  $E$  **do**
  - 4:   **for** step = 1 to  $T$  **do**
  - 5:     Sequentially select a parameter combination  $pc = (K, p_{\max}, Q)$  from  $\mathcal{C}$
  - 6:     Sample a batch of  $B$  problem instances  $s$  with fixed  $pc$
  - 7:     For each  $s$ : sequentially select secondary starting nodes from  $N$ ; generate rollout sequences  $\Pi$  via the  $\theta$ -parameterized AEDM
  - 8:     Normalize rewards using EMA with Z-score normalization
  - 9:     Compute shared baseline:  $b(s) = \frac{1}{|\Pi|} \sum_{\pi \in \Pi} R(\pi|s)$
  - 10:    Calculate policy gradient using (18)
  - 11:    Update  $\theta$  via Adam optimizer:  $\theta \leftarrow \text{Adam}(\theta, \nabla_\theta J(\theta))$
  - 12:   **end for**
  - 13: **end for**
  - 14: **Output:** Optimized AEDM parameters  $\theta$
- 

## 5.4. Instance generation

**5.4.1. Training instance generation** In contrast to prior DRL studies focused on combinatorial optimization problems such as vehicle routing problem (VRP) and traveling salesman problem (TSP) (Kool et al. 2018, Kwon et al. 2020, Luo et al. 2023, Liu et al. 2024a, Berto et al. 2024)—which generate training instances via random node placement in a coordinate system—our

drone routing problem requires road network-based instances. Given the scarcity of public road network datasets (fewer than 20, e.g., <https://github.com/bstabler/TransportationNetworks>), insufficient for effective DRL training, we propose a synthetic road network generation method.

Upon the occurrence of a disaster, the real-world road network  $G = (N, A)$  is known, including the latitude and longitude of each node  $N$ , and the length of each link  $A$ . We can convert latitude and longitude coordinates to planar projection coordinates. These coordinates are subsequently subjected to center translation and equidistant regularization to achieve uniform normalization within the range  $[0, 1]^2$ , thereby preserving the proportional relationships of original distances post-normalization. Training instances are generated as follows:

- a) **Grid Network Initialization:** A uniform square grid of  $N$  nodes is created over  $[0, 1]^2$  (see Figure 7 (a)).
- b) **Link Pruning:** Randomly remove edge subsets (prioritizing boundary nodes) while maintaining connectivity, resulting in  $A$  edges (see Figure 7 (b)).
- c) **Node Perturbation:** Introduce bounded random perturbations to node coordinates to avoid regularity, ensuring no overlaps and confinement to  $[0, 1]^2$  (see Figure 7 (c)).
- d) **Attribute Assignment:** Compute Euclidean lengths for remaining edges, scaled by  $[1, 2]$  to simulate real-world road distances. Using the transformation in Section 4, convert to a node-based network with artificial node coordinates. Randomly sample damage information values  $c_p$ , serving as the reward signal during training.

This method generates large-scale, diverse, and realistic road network instances—addressing dataset scarcity and enabling effective DRL training for disaster-response drone routing.

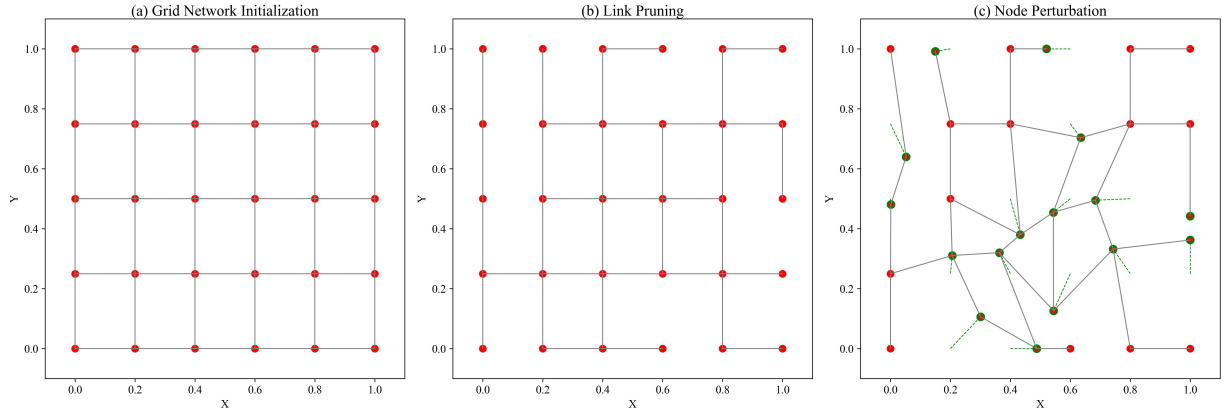


**Figure 7** The three-stage synthetic road network generation for drone routing training. (a) Initializes a  $N = 30$  node grid in  $[0, 1]^2$ . (b) Prunes edges (prioritizing boundaries) to retain  $A = 36$  edges while ensuring connectivity, mimicking real-world sparsity. (c) Applies bounded random node perturbations within  $[0, 1]^2$  to break regularity and introduce topological diversity. This pipeline addresses dataset scarcity, enabling realistic training environments for DRL-based drone routing optimization.

**5.4.2. Testing instance generation** Given the transformed road network structure, we select  $N$  nodes as the secondary visit set for drones. A critical limitation of POMO’s multi-greedy inference for our problem is that  $N$  (the number of greedy rollouts) cannot scale arbitrarily. Inspired by data augmentation in computer vision (e.g., cropping and flipping) and natural language processing (e.g., back-translation), Kwon et al. (2020) proposed generating new instances via coordinate transformations.

For our problem, we apply a similar strategy. We perform 8-fold augmentations on the node coordinates  $(x_i, y_i)$  in the transformed network. These augmentations include flipping along the x-axis, y-axis, and their combinations, generating eight distinct yet equivalent problem instances. Specifically, the transformations are: keeping the original coordinates  $[x, y]$ ; flipping the x-coordinate to get  $[1 - x, y]$ ; flipping the y-coordinate to get  $[x, 1 - y]$ ; flipping both coordinates to get  $[1 - x, 1 - y]$ ; swapping coordinates to get  $[y, x]$ ; swapping and flipping the y-coordinate to get  $[1 - y, x]$ ; swapping and flipping the x-coordinate to get  $[y, 1 - x]$ ; and swapping and flipping both coordinates to get  $[1 - y, 1 - x]$ .

This method preserves the solution space, ensuring interchangeability between original and augmented instances. While previous works (Kwon et al. 2020, Luo et al. 2023, Berto et al. 2024) explored additional transformations (e.g., rotations), we prioritize simplicity and omit these for this study. Future work may investigate their potential to further enhance model performance.

## 6. Experiments

### 6.1. Experiment setting

**Model Parameters.** AEDM is trained with an embedding size  $d = 128$ . Its encoder consists of  $l = 6$  layers with 8-head MHA and FFN hidden size 512. These parameters choices are informed by successful applications for learning-based methods in solving traditional TSP and VRP (Kool et al. 2018, Kwon et al. 2020, Luo et al. 2023, Zhou et al. 2024, Liu et al. 2024a, Berto et al. 2024). This configuration yields about 1.3 million trainable parameters. Training spans 200 epochs (batch size = 64) on 10,000 on-the-fly generated instances. The Adam optimizer uses an initial learning rate of  $10^{-4}$ ,  $L_2$  regularization ( $10^{-6}$  weight decay), and learning rate decay ( $\times 0.1$  at epochs 190).

**Problem Parameters.** AEDM is trained on 100-node instances, comprising 50 nodes in set  $\mathcal{P}$  (with damage information values, representing 50 assessable road links) and 50 nodes in set  $N$  (without damage information, including one depot). Generalization is evaluated on larger instances (200, 400, 600, 800, and 1,000 nodes), each with 50% nodes in  $\mathcal{P}$  and 50% in  $N$ . Damage values for  $\mathcal{P}$  are uniformly sampled from  $[1, 10]$  and normalized by dividing by 10. Training uses 2, 3, or 4 drones. Practically, drones have a 2-hour battery flight time limit  $Q$  and a speed of 60 km/h (Zhang et al. 2023). Given the time-critical nature of disaster response, assessment time limits

$p_{\max}$  are set to 30, 45, and 60 minutes (corresponding to 30, 45, and 60 km flight distances). Since  $Q$  is significantly larger than  $p_{\max}$ , and drone flight time being less than  $p_{\max}$  inherently implies it is less than  $Q$ ,  $Q$  is not considered in subsequent experiments, with focus on  $p_{\max}$ . Road network coordinates are normalized to  $[0, 1]$ , with link lengths scaled accordingly. For simplified data generation, training uses  $p_{\max} = 2, 3, 4$  corresponding to 30, 45, and 60 minutes in real-world distances.

**Training time.** Training is conducted on Google Colab using an NVIDIA A100 GPU. Each epoch requires approximately 1 minute, resulting in a total training duration of around 3.33 hours for 200 epochs.

## 6.2. Benchmark

The proposed problem is novel, with no existing exact or heuristic algorithms tailored to it. For comparison, we developed a mathematical model (detailed in Appendix 7) and solved it using commercial solvers (e.g., Gurobi)—a method, like AEDM, that requires no domain knowledge for algorithm design. However, formulating a fully corresponding model for this new problem is complex, demanding domain expertise and significant time investment (see Appendix 7).

Given the time sensitivity of disaster response, both solution quality and speed are critical, and we compare both metrics. Notably, disaster scenarios require assessing road networks across multiple locations (e.g., post-earthquake or flood), meaning problem instances to solve are not singular but multiple. Thus, both AEDM and Gurobi must handle multiple instances simultaneously. AEDM leverages GPU parallelism to process up to 1,000 instances per run—consistent with prior applications in combinatorial optimization (e.g., TSP and VRP) (Kool et al. 2018, Kwon et al. 2020, Luo et al. 2023, Zhou et al. 2024, Liu et al. 2024a, Berto et al. 2024). While Gurobi supports parallelization across CPU cores (Zhou et al. 2024, Berto et al. 2024), our experiments—consistent with common real-world deployment constraints due to CPU setup limitations—did not utilize this parallelization for Gurobi. To ensure fairness and reliability despite this constraint, all results are averaged over 10 problem instances for both AEDM and Gurobi. Specifically, AEDM’s total computation time across the 10 instances is reported, while Gurobi’s average time per instance is used—placing Gurobi in an advantageous position, though this does not affect AEDM’s performance.

## 6.3. Computational performance

Table 2 and Table 3 compare results across varying numbers of drones in a fixed 200-node network, with the maximum allowable time  $p_{\max}$  set to 30 and 45 minutes, respectively. Table 4 and Table 5 present analogous comparisons for a fixed 400-node network under the same  $p_{\max}$  values, with drone numbers varied. In each table, the first column lists the names of the methods, where

**Table 2 Performance Comparison of Methods in 200-Node Network ( $p_{\max} = 30$  min, Varying Drones)**

Method	#Drone	Time (s)	Value	Gap	#Drone	Time (s)	Value	Gap
Gurobi	2	100	11.90	24.23%	3	100	12.73	40.78%
		500	13.62	13.29%		500	16.49	23.31%
		1,000	14.57	7.26%		1,000	19.10	11.13%
		2,000	15.31	2.54%		2,000	21.04	2.14%
AEDM	1	15.07	4.04%		1	20.60	4.18%	
AEDM $\times$ 8	1	15.71	0.00%		1	21.50	0.00%	
Gurobi	4	100	15.59	40.62%	5	100	15.62	51.80%
		500	20.08	23.50%		500	22.80	29.62%
		1,000	20.08	23.50%		1,000	22.80	29.62%
		2,000	20.78	20.84%		2,000	24.32	24.92%
AEDM	1	25.12	4.30%		1	31.28	3.45%	
AEDM $\times$ 8	1	26.25	0.00%		1	32.39	0.00%	

**Table 3 Performance Comparison of Methods in 200-Node Network  $p_{\max} = 45$  min, Varying Drones)**

Method	#Drone	Time (s)	Value	Gap	#Drone	Time (s)	Value	Gap
Gurobi	2	100	13.40	44.39%	3	100	21.55	33.61%
		500	22.02	8.58%		500	26.82	17.37%
		1,000	22.05	8.45%		1,000	26.82	17.37%
		2,000	22.33	7.29%		2,000	27.82	14.28%
AEDM	1	23.34	3.12%		1	31.33	3.49%	
AEDM $\times$ 8	1	24.09	0.00%		1	32.46	0.00%	
Gurobi	4	100	27.62	30.32%	5	100	23.80	47.00%
		500	31.97	19.34%		500	34.36	23.47%
		1,000	31.97	19.34%		1,000	34.56	23.03%
		2,000	31.97	19.34%		2,000	34.76	22.58%
AEDM	1	38.30	3.39%		1	43.29	3.58%	
AEDM $\times$ 8	1	39.64	0.00%		1	44.90	0.00%	

**Table 4 Performance Comparison of Methods in 400-Node Network ( $p_{\max} = 30$  min, Varying Drones)**

Method	#Drone	Time (s)	Value	Gap	#Drone	Time (s)	Value	Gap
Gurobi	2	100	-	100.00%	3	100	-	100.00%
		500	10.22	59.59%		500	11.14	66.63%
		1,000	18.61	26.44%		1,000	21.67	35.11%
		2,000	22.20	12.26%		2,000	27.79	16.76%
AEDM	1	24.30	3.95%		1	32.06	3.98%	
AEDM $\times$ 8	1	25.30	0.00%		1	33.39	0.00%	
Gurobi	4	100	-	100.00%	5	100	-	100.00%
		500	17.06	58.32%		500	12.43	73.74%
		1,000	21.47	47.56%		1,000	29.10	38.53%
		2,000	33.85	17.32%		2,000	35.64	24.72%
AEDM	1	39.00	4.73%		1	44.91	5.12%	
AEDM $\times$ 8	1	40.94	0.00%		1	47.34	0.00%	

**Table 5 Performance Comparison of Methods in 400-Node Network ( $p_{\max} = 45$  min, Varying Drones)**

Method	#Drone	Time (s)	Value	Gap	#Drone	Time (s)	Value	Gap
Gurobi	2	100	-	100.00%	3	100	-	100.00%
		500	27.88	31.31%		500	27.65	45.21%
		1,000	31.41	22.63%		1,000	37.30	26.06%
		2,000	34.83	14.19%		2,000	42.89	14.99%
AEDM		1	38.96	4.03%		1	48.42	4.04%
AEDM $\times$ 8		1	40.59	0.00%		1	50.45	0.00%
Gurobi	4	100	-	100.00%	5	100	-	100.00%
		500	29.19	52.25%		500	27.39	60.49%
		1,000	44.08	27.88%		1,000	43.28	37.58%
		2,000	48.99	19.85%		2,000	51.94	25.09%
AEDM		2	58.28	4.66%		2	64.31	7.24%
AEDM $\times$ 8		2	61.13	0.00%		2	69.33	0.00%

AEDM  $\times$  8 denotes the proposed model with  $8 \times$  instance augmentation during testing. The second column indicates the number of drones; the third column reports solution time, where Gurobi's values correspond to its maximum allowed solving time—set to 100, 500, 1,000, and 2,000 seconds to reflect disaster response time constraints. The fourth column shows the optimal objective value at the recorded time, and the fifth column presents the gap, defined as  $\text{Gap} = (y - y_{\text{other}})/y$ , where  $y$  is the objective value from AEDM  $\times$  8 and  $y_{\text{other}}$  from other methods. The comparative results reveal three critical insights:

a) Solution Quality: AEDM Outperforms Gurobi Across Scales

Across all node numbers,  $p_{\max}$  values, and drone numbers, AEDM and AEDM  $\times$  8 yield higher objective values than Gurobi. For 200-node networks (Table 2–Table 3), Gurobi's solutions show gaps of 2.14–47% relative to AEDM  $\times$  8. For larger 400-node networks (Table 4–Table 5), Gurobi's gaps widen to 12.26–100%, with complete failures in early time windows. Figure 8 visually analyzes these performance gaps across parameter combinations via radar and box-plot charts, confirming AEDM  $\times$  8's consistent superiority across all metrics, followed by AEDM with minor positive gaps, and Gurobi with the largest deficits.

b) Computational Efficiency: AEDM Meets Urgent Time Constraints, Gurobi Lags

AEDM and AEDM  $\times$  8 achieve inference in 1–2 seconds across all instances, aligning with the urgent time constraints of disaster response. In contrast, Gurobi requires significantly longer computation time (100–2,000 seconds) and fails to produce valid solutions within 100 seconds for 400-node networks (marked by “-” in Table 4 and Table 5).

c) Instance Augmentation Enhances Performance

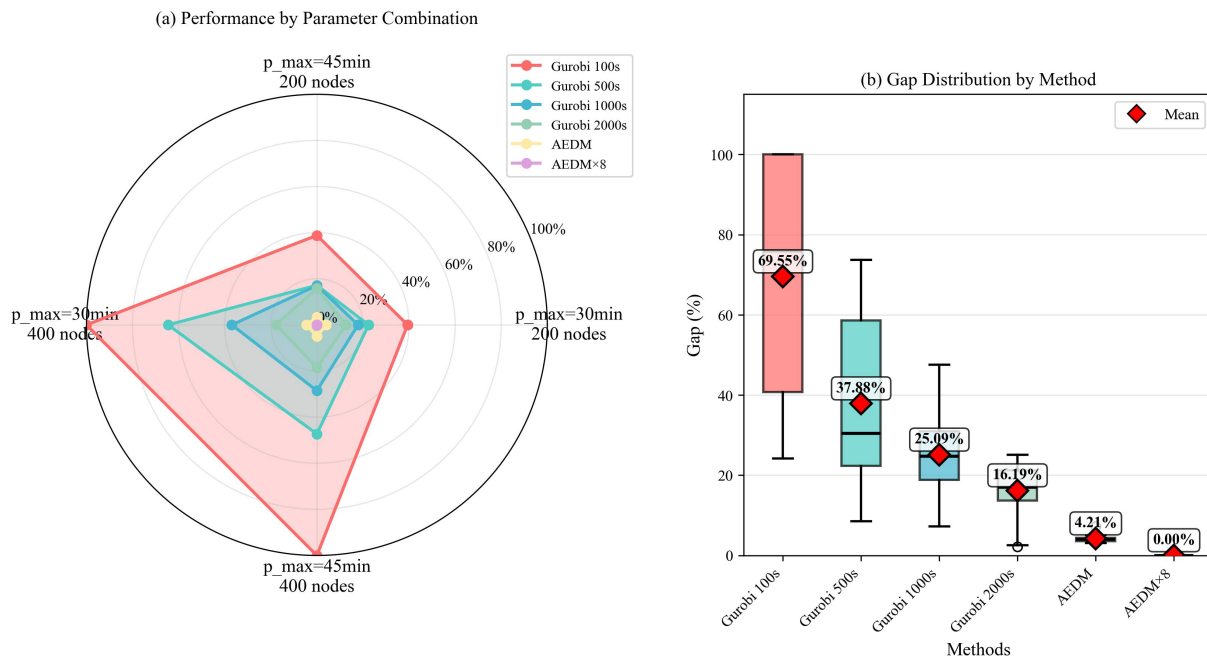
AEDM  $\times$  8 consistently outperforms the base AEDM, with objective value gaps of 3.12–7.24% across all scenarios, demonstrating that instance augmentation effectively boosts performance.

In summary, AEDM and its augmented variant (AEDM  $\times$  8) emerge as superior solutions for post-disaster road damage assessment, offering unparalleled speed and quality compared to traditional solvers like Gurobi, with instance augmentation further enhancing performance.

#### 6.4. Method robustness

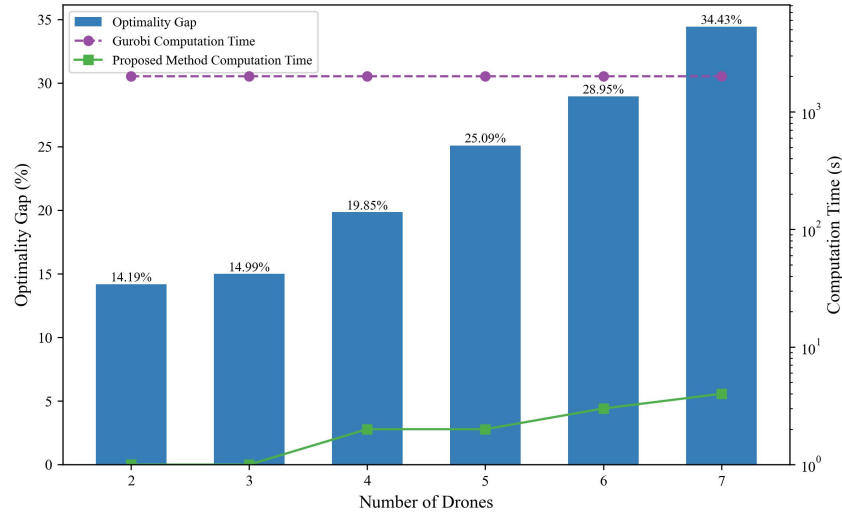
We further analyze the robustness of AEDM by testing it on parameter distributions that were not seen during training. Figure 9 assesses AEDM's generalization across drone numbers (2–7), where 2–4 were training-seen and 5–7 were unseen. Gurobi operates within a fixed 2,000-second time limit for all cases. In contrast, AEDM completes real-time optimization across all drone numbers: it maintains high efficiency for training-seen ranges (2–4) and retains fast computation with strong objective values for unseen ranges (5–7). This confirms AEDM's robustness: it generalizes to unseen distributions, sustaining efficiency and solution quality as problem complexity (unseen drone numbers) increases, outperforming Gurobi's time-constrained, quality-degrading performance.

Figure 10 assesses AEDM's robustness across varying maximum allowable assessment time ( $p_{\max}$ ), including 30, 45, and 60 minutes (seen during training) as well as 75, 90, and 105 minutes (held out as unseen). The experimental setup fixes nodes at 400 and drones at 4. As shown in the figure, Gurobi hits a fixed 2,000-second time limit across all  $p_{\max}$  settings. In contrast, AEDM completes real-time optimization for all  $p_{\max}$  values: it maintains efficiency for training-seen ranges (30–60 minutes) and retains fast computation for unseen ranges (75–105 minutes). Meanwhile, the optimality gap between AEDM and Gurobi widens with increasing  $p_{\max}$  (from 17.32% at 30



**Figure 8** Performance Comparison: Average Gap (%) by Method Different Parameter Combinations





**Figure 9** Sensitivity Analysis with Varying Numbers of Drones; Fixed Node of 400 and  $p_{\max} = 45$

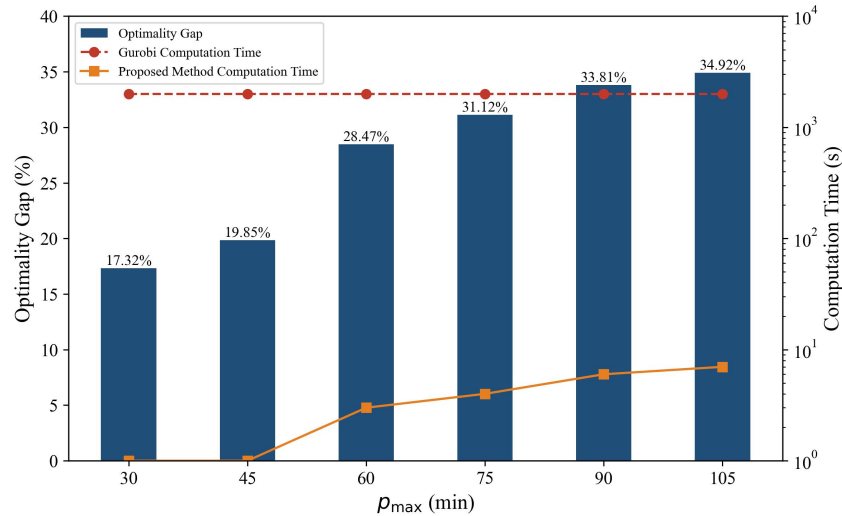


**Figure 10** Sensitivity Analysis with Varying Maximum Allowable Time ( $p_{\max}$ ); Fixed Node of 400 and 4 Drones

minutes to 34.92% at 105 minutes). This confirms AEDM's robustness: it generalizes to unseen  $p_{\max}$  distributions, sustaining efficiency and solution quality as temporal complexity increases and outperforming Gurobi's time-bound, quality-degrading behavior.

Figure 11 assesses AEDM's robustness on unseen node scales (200–1,000 nodes), with drones fixed at 4 and  $p_{\max} = 45$ . As shown in the figure, for smaller, training-relevant scales (200–400 nodes), AEDM completes real-time optimization. For large, unseen scales (600–1,000 nodes), Gurobi fails to return feasible solutions within the 2,000-second limit (100% time-out gaps, gray bars). In contrast, AEDM still finalizes optimization in real-time, sustaining efficiency even as node number increases. This confirms AEDM's superiority: it generalizes to large, unseen network scales, maintaining

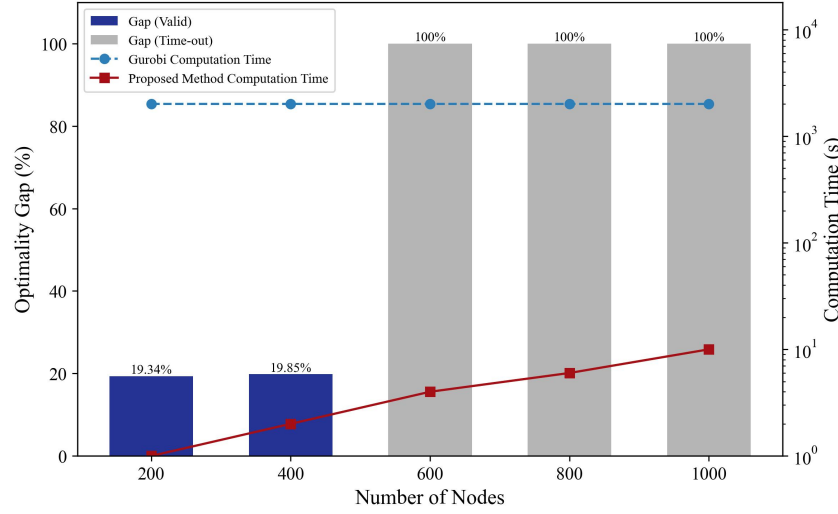


**Figure 11** Sensitivity Analysis with Varying Node Sizes; Fixed  $p_{\max} = 45$  and 4 Drones

computational feasibility and solution quality. Traditional solvers like Gurobi collapse under scale, highlighting AEDM's critical advantage for large-scale road network assessments.

In summary, this section evaluates AEDM's robustness across unseen parameter distributions. Tests on drone numbers, assessment time limits, and node scales show that unlike Gurobi—limited by long computation time and deteriorating results—AEDM sustains efficiency and quality, proving its superiority for time-critical, large-scale road network assessment tasks.

### 6.5. Real-world application

To validate AEDM's performance on realistic road networks, we conduct experiments using a publicly available transportation network from the transportation networks (<https://github.com/bstabler/TransportationNetworks>), which represents a large-scale and complex scenario typical in post-disaster assessment. The Anaheim network (416 nodes, 914 links) serves as a metropolitan transportation system, approximating the complexity of city-wide post-disaster road damage assessment, as shown in Figure 12. Following the coordinate normalization procedure described in Section 5.4.1, we convert the geographical coordinates (latitude and longitude) of the network to planar projection coordinates, then apply center translation and equidistant regularization to achieve uniform normalization within  $[0, 1]^2$ . For Anaheim, we test drone numbers  $K \in \{5, 6, 7\}$  and the maximum allowable assessment time  $p_{\max} \in \{30, 45, 60\}$  minutes with Gurobi's time limit extended to 10,000 seconds due to increased problem complexity. Figure 13 presents scatter plots comparing AEDM and Gurobi performance across all parameter combinations, with computation time on the x-axis and objective value on the y-axis, demonstrating AEDM's superiority in both solution quality and computational efficiency. For solution quality, AEDM consistently outperforms Gurobi with gaps of 11.67–24.68% for Anaheim, while for computational efficiency,

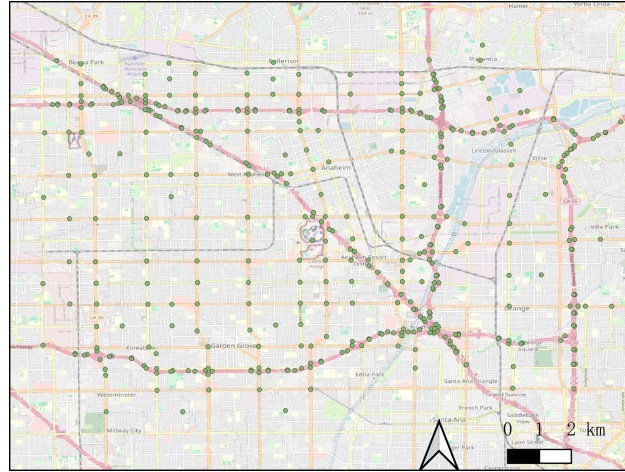


**Figure 12** Anaheim road network

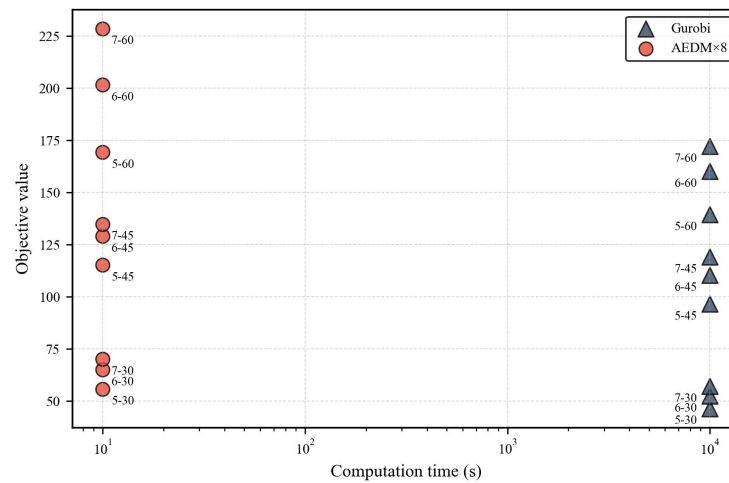


**Figure 13** Performance Comparison Between AEDM and Gurobi on Anaheim Road Network

AEDM achieves real-time performance with approximately 10 seconds, compared to Gurobi's full allocated time limit of 10,000 seconds without guarantee of optimal solutions. These results confirm AEDM's practical applicability for time-critical disaster response scenarios, where both solution quality and rapid deployment are essential.

## 7. Conclusion

This study addresses the challenge of rapid post-disaster road network damage assessment through drone routing optimization. We propose AEDM that determines high-quality drone assessment routes in real-time without requiring domain-specific algorithmic expertise. The key contributions include: (1) AEDM achieves superior performance compared to commercial solvers, with solution quality improvements of 16–69% while maintaining real-time inference (1–2 seconds vs. 100–2,000 seconds for traditional methods); (2) A simple yet effective network transformation

approach that converts a link-based routing problem into an equivalent node-based formulation; (3) A synthetic road network generation method that addresses the scarcity of large-scale training datasets for DRL applications. Experimental results demonstrate AEDM’s robustness across varying problem scales, drone numbers, and time constraints, with consistent generalization to unseen parameter distributions. The model’s ability to balance computational efficiency with solution quality makes it particularly suitable for time-critical disaster response scenarios where rapid decision-making is essential.

Future research can pursue two directions. First, while the proposed multi-task model addresses scenarios with multiple drone numbers and assessment time limits, it can be extended to accommodate more complex road damage assessment scenarios by integrating diverse constraints—including multiple depots, time windows for individual road links, and route “open/closed” assessment status. We plan to develop a unified model to tackle a broader spectrum of road damage assessment problems. Second, drawing on the scaling law in large language models, where performance improves with parameter size (currently reaching billions) (Achiam et al. 2023, Touvron et al. 2023, Guo et al. 2025), we aim to investigate whether increasing the parameter count of our model can further enhance its performance.

## References

- Abuali, T.M., Ahmed, A.A., 2025. Innovative applications of swarm drones in disaster management and rescue operations. *The Open European Journal of Engineering and Scientific Research* , 23–31.
- Achiam, J., Adler, S., Agarwal, S., Ahmad, L., Akkaya, I., Aleman, F.L., Almeida, D., Altenschmidt, J., Altman, S., Anadkat, S., et al., 2023. Gpt-4 technical report. *arXiv preprint arXiv:2303.08774* .
- Adsanver, B., Coban, E., Balcik, B., 2025. A predictive multistage postdisaster damage assessment framework for drone routing. *International Transactions in Operational Research* 32, 626–668.
- Agatz, N., Bouman, P., Schmidt, M., 2018. Optimization approaches for the traveling salesman problem with drone. *Transportation Science* 52, 965–981.
- Arishi, A., Krishnan, K., 2023. A multi-agent deep reinforcement learning approach for solving the multi-depot vehicle routing problem. *Journal of Management Analytics* 10, 493–515.
- Avishan, F., Elyasi, M., Yanıkoğlu, İ., Ekici, A., Özener, O.Ö., 2023. Humanitarian relief distribution problem: An adjustable robust optimization approach. *Transportation Science* 57, 1096–1114.
- Balcik, B., 2017. Site selection and vehicle routing for post-disaster rapid needs assessment. *Transportation Research Part E: Logistics and Transportation Review* 101, 30–58.
- Balcik, B., Yanıkoğlu, İ., 2020. A robust optimization approach for humanitarian needs assessment planning under travel time uncertainty. *European Journal of Operational Research* 282, 40–57.

- Baldacci, R., Maniezzo, V., 2006. Exact methods based on node-routing formulations for undirected arc-routing problems. *Networks* 47, 52–60.
- Bello, I., Pham, H., Le, Q.V., Norouzi, M., Bengio, S., 2016. Neural combinatorial optimization with reinforcement learning. *arXiv preprint arXiv:1611.09940* .
- Berto, F., Hua, C., Zepeda, N.G., Hottung, A., Wouda, N., Lan, L., Park, J., Tierney, K., Park, J., 2024. Routefinder: Towards foundation models for vehicle routing problems. *arXiv preprint arXiv:2406.15007* .
- Boyles, S.D., Lownes, N.E., Unnikrishnan, A., 2023. *Transportation Network Analysis*. volume 1. Edition 0.91.
- Bravo, R.Z.B., Leiras, A., Cyrino Oliveira, F.L., 2019. The use of uavs in humanitarian relief: An application of pomdp-based methodology for finding victims. *Production and Operations Management* 28, 421–440.
- Brown, T., Mann, B., Ryder, N., Subbiah, M., Kaplan, J.D., Dhariwal, P., Neelakantan, A., Shyam, P., Sastry, G., Askell, A., et al., 2020. Language models are few-shot learners. *Advances in Neural Information Processing Systems* 33, 1877–1901.
- Chen, X., Ulmer, M.W., Thomas, B.W., 2022. Deep q-learning for same-day delivery with vehicles and drones. *European Journal of Operational Research* 298, 939–952.
- Enayati, S., Li, H., Campbell, J.F., Pan, D., 2023. Multimodal vaccine distribution network design with drones. *Transportation Science* 57, 1069–1095.
- Glock, K., Meyer, A., 2020. Mission planning for emergency rapid mapping with drones. *Transportation Science* 54, 534–560.
- Gunawan, A., Lau, H.C., Vansteenwegen, P., 2016. Orienteering problem: A survey of recent variants, solution approaches and applications. *European Journal of Operational Research* 255, 315–332.
- Guo, D., Yang, D., Zhang, H., Song, J., Zhang, R., Xu, R., Zhu, Q., Ma, S., Wang, P., Bi, X., et al., 2025. Deepseek-r1: Incentivizing reasoning capability in llms via reinforcement learning. *arXiv preprint arXiv:2501.12948* .
- He, K., Zhang, X., Ren, S., Sun, J., 2016. Identity mappings in deep residual networks, in: *Computer Vision–ECCV 2016: 14th European Conference, Amsterdam, The Netherlands, October 11–14, 2016, Proceedings, Part IV* 14, Springer. pp. 630–645.
- Huang, C., Tang, Z., Hu, S., Jiang, R., Zheng, X., Ge, D., Wang, B., Wang, Z., 2025. Orlm: A customizable framework in training large models for automated optimization modeling. *Operations Research* .
- Huang, M., Smilowitz, K.R., Balcik, B., 2013. A continuous approximation approach for assessment routing in disaster relief. *Transportation Research Part B: Methodological* 50, 20–41.
- Kool, W., Van Hoof, H., Welling, M., 2018. Attention, learn to solve routing problems! *arXiv preprint arXiv:1803.08475* .

- Kwon, Y.D., Choo, J., Kim, B., Yoon, I., Gwon, Y., Min, S., 2020. Pomo: Policy optimization with multiple optima for reinforcement learning. *Advances in Neural Information Processing Systems* 33, 21188–21198.
- Liu, F., Lin, X., Wang, Z., Zhang, Q., Xialiang, T., Yuan, M., 2024a. Multi-task learning for routing problem with cross-problem zero-shot generalization, in: *Proceedings of the 30th ACM SIGKDD Conference on Knowledge Discovery and Data Mining*, pp. 1898–1908.
- Liu, F., Tong, X., Yuan, M., Lin, X., Luo, F., Wang, Z., Lu, Z., Zhang, Q., 2024b. Evolution of heuristics: Towards efficient automatic algorithm design using large language model. *arXiv preprint arXiv:2401.02051* .
- Liu, Z., Li, X., Khojandi, A., 2022. The flying sidekick traveling salesman problem with stochastic travel time: A reinforcement learning approach. *Transportation Research Part E: Logistics and Transportation Review* 164, 102816.
- Longo, H., De Aragao, M.P., Uchoa, E., 2006. Solving capacitated arc routing problems using a transformation to the cvrp. *Computers & Operations Research* 33, 1823–1837.
- Luo, F., Lin, X., Liu, F., Zhang, Q., Wang, Z., 2023. Neural combinatorial optimization with heavy decoder: Toward large scale generalization. *Advances in Neural Information Processing Systems* 36, 8845–8864.
- Maya, A., 2013. Rapid assessment in disasters. *JMAJ* 56, 19–24.
- Miller, C.E., Tucker, A.W., Zemlin, R.A., 1960. Integer programming formulation of traveling salesman problems. *Journal of the ACM (JACM)* 7, 326–329.
- Morandi, N., Leus, R., Yaman, H., 2024. The orienteering problem with drones. *Transportation Science* 58, 240–256.
- Organization, W.H., et al., 2000. Natural disasters: protecting the public’s health, in: *Natural disasters: protecting the public’s health*, pp. 119–119.
- Oruc, B.E., Kara, B.Y., 2018. Post-disaster assessment routing problem. *Transportation Research Part B: Methodological* 116, 76–102.
- Pearn, W.L., 1988. New lower bounds for the capacitated arc routing problem. *Networks* 18, 181–191.
- Radford, A., Kim, J.W., Hallacy, C., Ramesh, A., Goh, G., Agarwal, S., Sastry, G., Askell, A., Mishkin, P., Clark, J., et al., 2021. Learning transferable visual models from natural language supervision, in: *International conference on machine learning*, PmLR. pp. 8748–8763.
- Shi, Y., Yang, J., Han, Q., Song, H., Guo, H., 2024. Optimal decision-making of post-disaster emergency material scheduling based on helicopter–truck–drone collaboration. *Omega* 127, 103104.
- Steenbergen, R.M., Van Heeswijk, W.J., Mes, M., 2025. The stochastic dynamic postdisaster inventory allocation problem with trucks and uavs. *Transportation Science* 59, 360–390.

- Sun, H., Li, J., Wang, T., Xue, Y., 2022. A novel scenario-based robust bi-objective optimization model for humanitarian logistics network under risk of disruptions. *Transportation Research Part E: Logistics and Transportation Review* 157, 102578.
- Tatham, P., 2009. An investigation into the suitability of the use of unmanned aerial vehicle systems (uavs) to support the initial needs assessment process in rapid onset humanitarian disasters. *International Journal of Risk Assessment and Management* 13, 60–78.
- Touvron, H., Lavril, T., Izacard, G., Martinet, X., Lachaux, M.A., Lacroix, T., Rozière, B., Goyal, N., Hambro, E., Azhar, F., et al., 2023. Llama: Open and efficient foundation language models. *arXiv preprint arXiv:2302.13971* .
- Turk, V., 2014. Drones mapped the philippines to improve typhoon aid efforts. *Motherboard*, May 9, 10.
- Vaswani, A., Shazeer, N., Parmar, N., Uszkoreit, J., Jones, L., Gomez, A., Kaiser, L., Polosukhin, I., 2017. Attention is all you need, in: *NIPS*.
- Yang, Y., Yin, Y., Wang, D., Ignatius, J., Cheng, T., Dhamotharan, L., 2023. Distributionally robust multi-period location-allocation with multiple resources and capacity levels in humanitarian logistics. *European Journal of Operational Research* 305, 1042–1062.
- Yin, Y., Yang, Y., Yu, Y., Wang, D., Cheng, T., 2023. Robust vehicle routing with drones under uncertain demands and truck travel times in humanitarian logistics. *Transportation Research Part B: Methodological* 174, 102781.
- Zhang, G., Jia, N., Zhu, N., Adulyasak, Y., Ma, S., 2023. Robust drone selective routing in humanitarian transportation network assessment. *European Journal of Operational Research* 305, 400–428.
- Zhang, K., He, F., Zhang, Z., Lin, X., Li, M., 2020. Multi-vehicle routing problems with soft time windows: A multi-agent reinforcement learning approach. *Transportation Research Part C: Emerging Technologies* 121, 102861.
- Zhou, J., Cao, Z., Wu, Y., Song, W., Ma, Y., Zhang, J., Xu, C., 2024. Mvmoe: Multi-task vehicle routing solver with mixture-of-experts. *arXiv preprint arXiv:2405.01029* .

## Appendices

### A. Derivation of point $C$ coordinates

Given points  $A(X_A, Y_A)$ ,  $B(X_B, Y_B)$ , and length  $L$ , we derive the coordinates  $C(X_C, Y_C)$  lying on  $AB$ 's perpendicular bisector with  $AC = L/2$  and  $CB = L/2$ .

First, compute the midpoint  $D$  and direction vectors:

$$D\left(\frac{X_A + X_B}{2}, \frac{Y_A + Y_B}{2}\right), \quad \vec{AB} = (X_B - X_A, Y_B - Y_A), \quad \vec{n} = (-(Y_B - Y_A), X_B - X_A) \quad (\text{A1})$$

The unit normal vector is:

$$\hat{n} = \left(\frac{-(Y_B - Y_A)}{d_{AB}}, \frac{X_B - X_A}{d_{AB}}\right), \quad \text{where } d_{AB} = \sqrt{(X_B - X_A)^2 + (Y_B - Y_A)^2} \quad (\text{A2})$$

Parametrize  $C$  along the bisector:

$$C = D + t\hat{n} \Rightarrow \begin{cases} X_C = \frac{X_A + X_B}{2} + t \frac{-(Y_B - Y_A)}{d_{AB}} \\ Y_C = \frac{Y_A + Y_B}{2} + t \frac{X_B - X_A}{d_{AB}} \end{cases} \quad (\text{A3})$$

Apply the length constraint  $AC = L/2$ :

$$\sqrt{\left(\frac{X_B - X_A}{2} - t \frac{Y_B - Y_A}{d_{AB}}\right)^2 + \left(\frac{Y_B - Y_A}{2} + t \frac{X_B - X_A}{d_{AB}}\right)^2} = \frac{L}{2} \quad (\text{A4})$$

Squaring and simplifying:

$$\frac{d_{AB}^2}{4} + t^2 = \frac{L^2}{4} \Rightarrow t = \pm \frac{\sqrt{L^2 - d_{AB}^2}}{2} \quad (\text{A5})$$

Substituting back yields the final coordinates:

$$X_C = \frac{X_A + X_B}{2} \mp \frac{\sqrt{L^2 - d_{AB}^2}}{2} \frac{Y_B - Y_A}{d_{AB}} \quad (\text{A6})$$

$$Y_C = \frac{Y_A + Y_B}{2} \pm \frac{\sqrt{L^2 - d_{AB}^2}}{2} \frac{X_B - X_A}{d_{AB}} \quad (\text{A7})$$

### B. Mathematical formulation

To formalize the problem, we define the binary decision variable  $x_{ij}^k$ , where  $x_{ij}^k = 1$  if drone  $k$  traverses road link  $(i, j)$  for assessment, and 0 otherwise. Using notations and network transformations from Sections 3 and 4, the drone-based road network assessment model is:

$$\max \sum_{k \in K} \sum_{p \in \mathcal{P}} c_p \left( \sum_{j: (p, j) \in \bar{A}} x_{pj}^k \right) \quad (\text{B1})$$

$$\text{s.t.} \quad \sum_{k \in K} \sum_{j: (p, j) \in \bar{A}} x_{pj}^k \leq 1 \quad \forall p \in \mathcal{P} \quad (\text{B2})$$

$$\sum_{j \in \bar{N}} x_{ji}^k = \sum_{j \in \bar{N}} x_{ij}^k \quad \forall i \in \bar{N}, \forall k \in K \quad (\text{B3})$$



$$\sum_{j \in \bar{N}} x_{oj}^k = \sum_{i \in \bar{N}} x_{io}^k = 1 \quad \forall k \in K \quad (\text{B4})$$

$$\sum_{(i,j) \in \bar{A}} t_{ij} x_{ij}^k \leq Q \quad \forall k \in K \quad (\text{B5})$$

$$\max_{k \in K} \left\{ \sum_{(i,j) \in \bar{A}} t_{ij} x_{ij}^k \right\} \leq p_{\max} \quad (\text{B6})$$

$$u_i^k + 1 - u_j^k \leq M(1 - x_{ij}^k) \quad \forall (i,j) \in \bar{A}, \forall k \in K \quad (\text{B7})$$

$$x_{ij}^k \in \{0, 1\} \quad \forall (i,j) \in \bar{A}, \forall k \in K \quad (\text{B8})$$

$$u_i^k \in \{1, 2, \dots, |\bar{N}|\} \quad \forall i \in \bar{N}, \forall k \in K \quad (\text{B9})$$

- Equation (B1) maximizes the total information value collected by all drones, summing  $c_p$  for each transformed artificial node traversed by drone  $k$  (as indicated by  $x_{ij}^k$ ).
- Constraints (B2) restrict each information-bearing artificial node to at most one drone visit, preventing redundant assessments by avoiding overlapping visits from multiple drones and thus ensuring assessment efficiency. Notably, this constraint does not impose a single-visit requirement on nodes within the original road network  $G$ , as illustrated in Figure 3.
- Constraints (B3) enforce flow conservation for each node  $i$  and drone  $k$ , ensuring equal entry and exit counts to maintain path continuity.
- Constraints (B4) require each drone  $k$  to start and end at depot  $o$ , with exactly one exit from and one entry to  $o$ .
- Constraints (B5) cap drone  $k$ 's total flight time (sum of  $t_{ij} x_{ij}^k$ ) at battery limit  $Q$ .
- Constraint (B6) ensures the maximum flight time across all drones does not exceed  $p_{\max}$ , enforcing timely completion of the entire assessment.

In the example in Figure 5, loops are valid and useful. Thus, unlike VRP and TSP, the loop-eliminating Miller-Tucker-Zemlin (MTZ) constraint would ideally be omitted here, as our problem allows loops in paths. However, model inspection reveals a critical issue: solving the model without such constraints yields discontinuous, invalid paths. To resolve this tension—enabling loops while ensuring path continuity—we initially proposed splitting nodes in  $N$  into three sub-nodes, with incoming/outgoing edges derived from the original node's edges. This approach, though, drastically increases node number and complicates solving. Consequently, consultation with domain modeling experts—itself a challenging and time-intensive process—was necessary, leading to a pragmatic decision: this model adopts the MTZ constraint. Specifically, the MTZ constraint in equation (B7) is utilized to preclude cycles or loops in the drone's path (Miller et al. 1960), enforced by a sufficiently large constant  $M$  (typically set to  $|\bar{N}|$ ). Auxiliary variables  $u_i^k$  ensure that if drone  $k$  travels from node  $i$  to node  $j$ , the path remains acyclic and continuous, thus avoiding node revisits. Finally,

equations (B8) and (B9) define the domains of decision variables:  $x_{ij}^k \in \{0, 1\}$  (binary indicator for whether drone  $k$  traverses link  $(i, j)$ ), and  $u_i^k \in \{1, 2, \dots, |\bar{N}|\}$  (integers representing the visit order of nodes by drone  $k$ ).

### C. Ablation study

To evaluate the impact of the proposed reward normalization strategy (EMA with Z-score normalization) on model performance, we conducted an ablation study by comparing four normalization variants of the AEDM framework:

- a) EMA with Z-score normalization: Combines EMA of both mean and variance to compute Z-score normalized rewards, as proposed in (15)-(17).
- b) Batch-wise Z-score normalization: Normalizes rewards within each batch using the batch mean and variance, without exponential smoothing.
- c) EMA mean division normalization: Normalizes rewards by dividing by the EMA of the mean (ignoring variance).
- d) No normalization: Uses raw rewards without any regularization.

All variants were trained under identical conditions detailed in Section 6.1 and evaluated on 400-node networks with  $p_{\max} = 45$  minutes and 4, 5, 6, 7 drones (i.e., four scenarios). Performance was quantified by the average optimality gap across these four scenarios, defined as  $\text{Gap} = (y - y_{\text{other}})/y$ . Here,  $y$  denotes the objective value from the EMA with Z-score normalization, and  $y_{\text{other}}$  represents that from other normalization variants. As visualized in Figure 14, the proposed reward normalization strategy achieves the best performance, whereas the “No normalization” variant yields the worst. These results underscore the critical role of EMA-based mean and variance tracking in stabilizing reinforcement learning for multi-task drone routing. The proposed normalization strategy ensures reward comparability across diverse parameter regimes (e.g., varying drone numbers and time limits), enabling effective model generalization to unseen scenarios.

### D. Method interpretability

To explore the model’s interpretability, we employ t-distributed stochastic neighbor embedding (t-SNE) to project high-dimensional representations—learned under varying drone numbers  $k$ ,  $p_{\max}$ , and a fixed 100-node scale—into a 2D space. With 100 instances per parameter combination, Figure 15 visualizes the evolution of features across the output of each encoder layer.

In Layer 1, features cluster distinctly by  $k$ - $p_{\max}$  combinations, indicating that the model first learns superficial parameter distinctions in initial layers and validating its ability to recognize input configurations. Progressing to Layer 2, clusters remain distinct but exhibit early fusion—features begin interacting across  $k$  and  $p_{\max}$  while retaining core differences. In Layers 3 and 4, clusters further soften and then mix: distributions of different  $k/p_{\max}$  values interweave, reducing strict

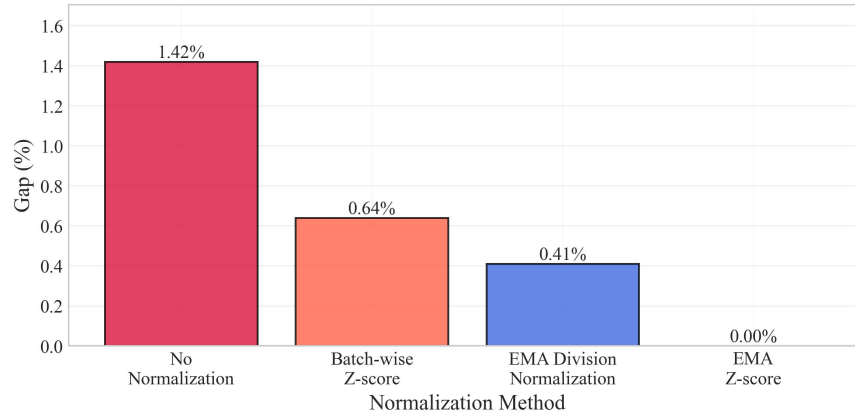


**Figure 14** Performance Gap of AEDM Under Diverse Reward Normalization Methods

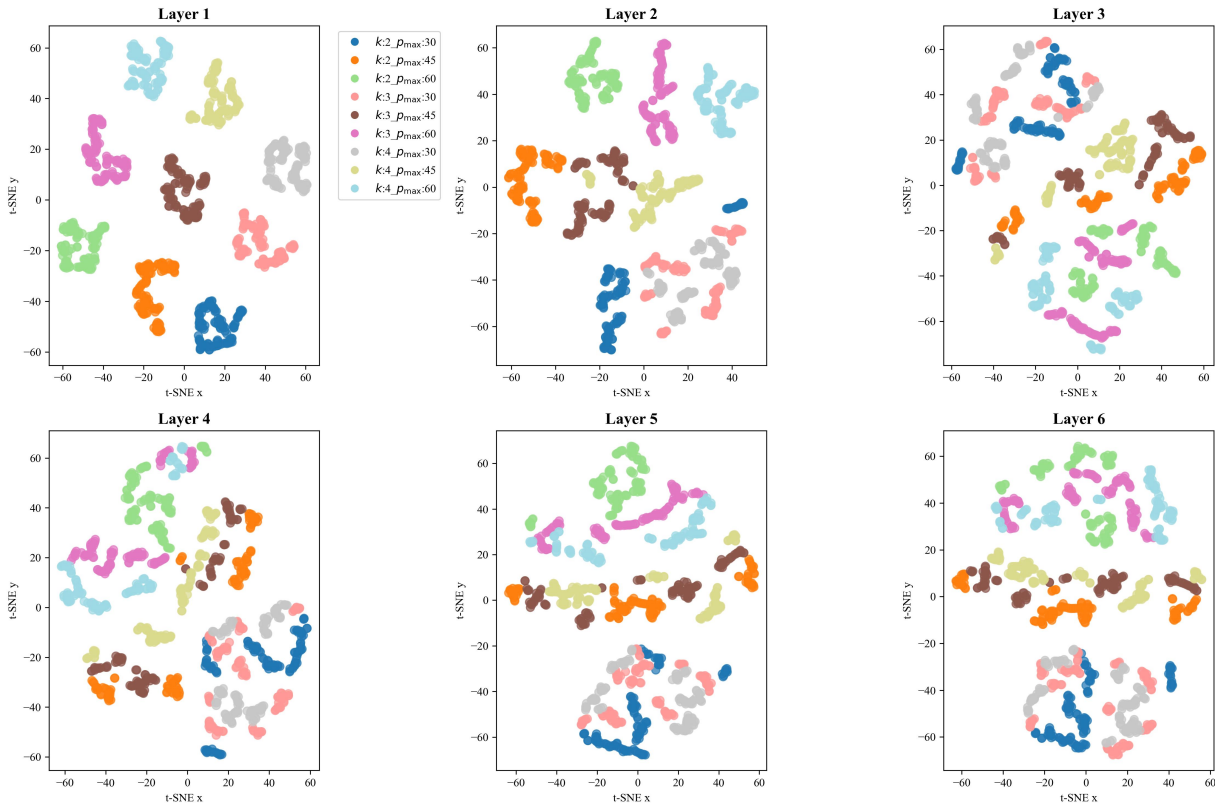


**Figure 15** Method Interpretability: Encoder Latent Space via Layer-Wise t-SNE Analysis

separation. In Layers 5 and 6, clusters dissolve into complex, interwoven distributions. This layer-by-layer t-SNE evolution reveals a clear learning trajectory: initial layers (1–2) recognize and separate raw input parameters ( $k$ ,  $p_{\max}$ ); middle layers (3–4) fuse these features; final layers (5–6) abstract core problem structures, prioritizing solution logics over input specifics. This confirms the model learns generalizable principles (not merely parameter patterns), leveraging the transformer architecture to distill raw inputs into abstract representations of the core problem. The cross-layer

feature fusion validates that the model transitions from “memorizing” to “reasoning”—a critical hallmark of effective problem-solving in complex tasks.